

# X-ray and soft $\gamma$ -ray spectra of Broad-Line Radio Galaxies

Przemysław R. Woźniak<sup>1,2</sup>, Andrzej A. Zdziarski<sup>2</sup>, David Smith<sup>3</sup>,  
Greg M. Madejski<sup>4,5</sup> and W. Neil Johnson<sup>6</sup>

<sup>1</sup>*Dept. of Astrophysical Sciences, Peyton Hall, Princeton University, Princeton, NJ 08544, USA*

<sup>2</sup>*N. Copernicus Astronomical Center, Bartycka 18, 00-716 Warsaw, Poland*

<sup>3</sup>*Dept. of Physics, University of Leicester, University Road, Leicester LE1 7RH, UK*

<sup>4</sup>*Lab for High Energy Astrophysics, NASA/GSFC, Greenbelt, MD 20771, USA*

<sup>5</sup>*Astronomy Dept., University of Maryland, College Park, MD 20742, USA*

<sup>6</sup>*E. O. Hulburt Center for Space Research, Naval Research Lab, Washington, DC 20375, USA*

Accepted 1998 May 1. Received 1997 April 5

## ABSTRACT

We study X-ray and soft  $\gamma$ -ray spectral properties of nearby Broad-Line Radio Galaxies (BLRGs) using data from *Ginga*, *ASCA*, OSSE and *EXOSAT*. The X-ray spectra are well fitted by an intrinsic power-law continuum with an energy index of  $\alpha \sim 0.7$ , moderately absorbed by a cold medium. In addition, the *Ginga* spectra show fluorescent Fe  $K\alpha$  lines with an average equivalent width of  $\sim 100$  eV, and, in some cases, Compton reflection humps. However, the latter components are significantly weaker than both those seen in radio-quiet Seyferts and those expected if the Fe  $K\alpha$  lines were due to reflection. We find that this weakness of reflection cannot be explained by dilution by another continuum component, e.g., from a jet. Some *ASCA* and *EXOSAT* spectra show soft X-ray excesses below  $\sim 3$  keV. When that component is taken into account, the Fe  $K\alpha$  lines in the *ASCA* data are found to be unresolved in most cases, and to have equivalent widths  $\lesssim 200$  eV, consistent with the *Ginga* data.

Multiple observations of 3C 390.3 and 3C 382 show the Fe  $K\alpha$  line approximately constant in flux but accompanied by strong continuum variations. This indicates the bulk of the line is formed by matter at a distance much larger than an accretion-disk scale, consistent with the *ASCA* line width measurements. The column density of the matter required to account for the observed line fluxes is  $N_{\text{H}} \gtrsim 10^{23}$  cm<sup>-2</sup>. Such a medium is in the line-of-sight in 3C 445 but it has to be out of it in other objects, in which the observed  $N_{\text{H}}$  are substantially lower. Thus, a cold medium with that  $N_{\text{H}}$  and covering a large solid angle is common in BLRGs but in most object it is out of the line-of-sight, consistent with the unified AGN model.

The spectra of BLRGs break and become softer above  $\sim 100$  keV, as shown by a simultaneous *ASCA*/OSSE observation of 3C 120 and by the OSSE spectra being on average much softer than the X-ray spectra. Finally, we find the X-ray and  $\gamma$ -ray spectral properties of Cen A, a bright narrow-line radio galaxy –  $\alpha \simeq 0.8$ , no or weak Compton reflection,  $N_{\text{H}} \gtrsim 10^{23}$  cm<sup>-2</sup> (which is consistent with the Fe  $K\alpha$  line flux), and a high-energy break at  $\sim 100$  keV – consistent with it being intrinsically very similar to BLRGs studied here, again in agreement with the unified model.

**Key words:** galaxies: active – galaxies: individual (3C 111, 3C 120, 3C 382, 3C 390.3, 3C 445, Cen A) – galaxies: Seyfert – gamma-rays: observations – line: profiles – X-rays: galaxies.

## 1 INTRODUCTION

The 2–20 keV X-ray spectra of Seyfert 1s have been studied using the *Ginga* data by Nandra & Pounds (1994, hereafter NP94). Those spectra have been found not to be simple power laws, but, instead, to show the presence of a charac-

teristic spectral upturn above  $\sim 10$  keV (see also Pounds et al. 1990), satisfactorily explained by Compton reflection from cold matter, presumably an accretion disk (Lightman & White 1988). However, NP94 have not distinguished in their study radio-quiet Seyferts from radio-loud ones, i.e. nearby broad-line radio galaxies (hereafter abbreviated as

BLRGs). On the other hand, Zdziarski et al. (1995, hereafter Z95) have found that two BLRGs observed by both *Ginga* and *CGRO/Oriented Scintillation Spectroscopy Experiment* (OSSE), 3C 111 and 3C 390.3, have the average spectrum with weak or no Compton reflection. That average spectrum is similar to the intrinsic spectrum of the nearby narrow-line radio galaxy Cen A, which also does not show Compton reflection (Miyazaki et al. 1996; Warwick, Griffiths & Smith 1998).

Here we study X-ray and soft  $\gamma$ -ray (hereafter abbreviated as  $X\gamma$ ) spectra of BLRGs observed by *Ginga*, *ASCA*, OSSE and *EXOSAT*. These radio-loud sources can be classified as Seyfert 1s using optical and UV lines and are listed as such by NP94. The morphology of most of the objects is consistent with elliptical (see Section 4). Our sample contains 5 BLRGs, of which 4 were observed by *Ginga*, 5 by *ASCA*, 3 by OSSE, and 5 by *EXOSAT*. Table 1 contains basic information on these objects. We selected the sources having radio to optical flux ratio  $F(5 \text{ GHz})/F(B \text{ optical}) \gg 10$  (Kellermann et al. 1989).

In Section 2 we describe the data used, and in Section 3 we present models used for the subsequent spectral fits. The results on individual objects are presented in Section 4. We specifically address the issues of the presence of the Compton reflection component and the strength and width of the fluorescence Fe  $K\alpha$  line. In Section 5, we discuss the average sample properties, the presence of breaks in soft  $\gamma$ -rays, and differences in X-ray spectral properties between BLRGs and radio-quiet Seyfert 1s. In Section 6, we consider the  $X\gamma$  spectra of the narrow-line radio galaxy Cen A, and compare them to those of our sample of BLRGs. In Section 7, we interpret our results, and summarize the main conclusions in Section 8.

## 2 THE DATA

For our study, we have selected BLRGs detected by either *Ginga*, *ASCA*, or OSSE. In addition, we consider observations of those objects by *EXOSAT*.

A total of 5 radio-loud Seyfert 1s were observed by *Ginga* LAC (the numbers of individual observations are given in brackets): 3C 98 [1], 3C 111 [1], 3C 382 [3], 3C 390.3 [2], and 3C 445 [1]. A rigorous data selection policy was adopted in order to exclude periods of high or unstable background (see, e.g., Smith & Done 1996). 3C 98 has not been detected and thus it is not included in our analysis. Table 2 contains the observation log for *Ginga*. The observations of 3C 111, 3C 382 and of the 1988 observation of 3C 390.3 are included in the sample of NP94, and of 3C382, 3C390.3, and 3C 445 in the sample of Lawson & Turner (1997).

The background was estimated using one of the two methods given by Hayashida et al. (1989) (see also Williams et al. 1992). The local method uses off-source observations taken within two days of (or at the same orbital phase as) the on-source observation to estimate the background level at the time of the observation, while the universal method uses all the off-source observations taken within a contemporary four month period to model systematic trends in the particle background levels, and hence to estimate the background level at the time of the source observation. It is found

that the universal method gave poor results for one observation of 3C 390.3 and all observations of 3C 382. For the remaining observations we used the results obtained from the universal method as it minimises the fluctuations in the cosmic X-ray background (Hayashida et al. 1989; Williams et al. 1992). For 3C 382 and 3C 445, the weakest of the sample, we have also added and subtracted a power law with  $\alpha = 0.8$  with the 1-keV normalization of  $5 \times 10^{-4} \text{ cm}^{-2} \text{ s}^{-1}$  (representing background fluctuations) to the data. The effect on the spectral slope below 10 keV was small,  $\pm 0.05$ , and completely negligible above 10 keV. Thus, we ignore this effect in fitting the data. Finally, due to the low Galactic latitude of 3C 111, the *Ginga* observation is possibly contaminated by the soft diffuse X-ray emission from our galaxy. To overcome this, we subtracted the best estimate of the local soft X-ray emission (derived from a nearby off-source observation) from the source data.

Data were then extracted from both the top-layer and mid-layer of the LAC, as the mid-layer has more effective area above  $\sim 10$  keV (although we ignore the mid-layer data below 10 keV as these are subject to greater uncertainties in background estimation). Contamination from fluorescence by silver atoms in the LAC collimator complicates the spectral analysis around  $\sim 22$  keV; for this reason, our analysis is restricted to the  $\sim 1.7$ –18 keV energy range. Prior to spectral fitting, the data were corrected for the collimator response and a 0.5 per cent systematic error was added to each PHA channel, to account for uncertainties in the detector response.

*ASCA* satellite consists of four co-aligned X-ray telescopes, and it covers a bandpass roughly from 0.4 to 10 keV (see Tanaka, Inoue & Holt 1994). The focal planes of two of the four telescopes have Gas Scintillation Imagers (GISs), while the remaining two have X-ray sensitive CCD cameras (Solid-state Imaging Spectrometers, or SISs), each consisting of four CCD detectors (chips). The observations of 3C 111 [1], 3C 120 [1], 3C 390.3 [3] and 3C 445 [1] were performed in a standard spectroscopy configuration with the source focussed on chip 1 in the SIS0 and on chip 3 in the SIS1. The observation of 3C 382 was performed with the source focussed on chip 2 in the SIS0 and on chip 0 in the SIS1 (a somewhat non-standard configuration). The log of the *ASCA* observations is given in Table 3.

The data were extracted from the HEASARC archives, and reduced using standard *ASCA* data reduction procedures. We used the *ASCA* rev. 2 processing, extracting manually the event files, but in the process of doing so, we used the standard screening criteria. In all cases, the SIS data presented here were analyzed in the highest spectral resolution “faint” mode, to assure that there would be no additional gain offset from the potential contamination by the scattered sunlight. For 3 objects, this results in a slightly lower effective observation time and thus slightly lower statistics than in the “bright” mode. However, there was no discernible difference between the results of the “faint” and “bright” mode spectral fits, as discussed in Section 4 below. On the other hand, the use of the “faint” mode for 3C 111 and 3C 382 resulted in only about 40 per cent of SIS0 data and 50 per cent of all SIS data, respectively, as compared to the “bright” mode. Therefore, in addition to the “faint” mode, we also performed the spectral fits to the data analyzed in

**Table 1.** The sample of BLRGs. The coordinates, redshifts, and Galactic column densities,  $N_{\text{H,G}}$  (in units of  $10^{21} \text{ cm}^{-2}$ ) are from Malaguti, Bassani & Caroli (1994). The NED database was used for the 5-GHz fluxes,  $F_{5 \text{ GHz}}$ . The extinction-corrected  $B$  magnitudes were taken from Smith & Heckman (1989) except for 3C 111, where we used the  $V$  magnitude from Brinkmann et al. (1995) and adopted  $B - V = 1.7$  from the AGN catalog of Véron-Cetty & Véron (1993).

Object	R.A.	Dec.	$z$	$N_{\text{H,G}}$	$F_{5 \text{ GHz}}/F_{\text{B}}$
3C 111	04 <sup>h</sup> 15 <sup>m</sup> 00 <sup>s</sup> .4	+37°54'16''	0.049	3.26	12400
3C 120	04 <sup>h</sup> 30 <sup>m</sup> 31 <sup>s</sup> .6	+05°15'00''	0.033	1.23	500
3C 382	18 <sup>h</sup> 33 <sup>m</sup> 12 <sup>s</sup> .0	+32°39'18''	0.058	0.79	400
3C 390.3	18 <sup>h</sup> 45 <sup>m</sup> 37 <sup>s</sup> .7	+79°43'06''	0.056	0.41	4300
3C 445	22 <sup>h</sup> 21 <sup>m</sup> 14 <sup>s</sup> .7	−02°21'25''	0.056	0.50	1100

**Table 2.** The observation log for *Ginga*. The count rate is for the top layer of the LAC in the 1.7–10 keV energy range. The uncertainties here and in Table 4 below correspond to 1- $\sigma$  confidence intervals.

Object	Start date	Start time	End date	End time	Exposure [s]	Count rate [ $\text{s}^{-1}$ ]
3C 111	1989-Feb-04	13:38:00	1989-Feb-05	11:00:00	18944	$12.42 \pm 0.06$
3C 382	1989-Jul-20	08:20:00	1989-Jul-21	00:35:00	15488	$5.51 \pm 0.08$
	1989-Jul-21	05:40:00	1989-Jul-21	22:50:00	17024	$5.13 \pm 0.09$
	1989-Jul-22	06:35:00	1989-Jul-24	00:00:00	30208	$5.16 \pm 0.06$
3C 390.3	1988-Nov-12	02:00:00	1988-Nov-14	03:00:00	46720	$17.40 \pm 0.06$
	1991-Feb-14	09:19:00	1991-Feb-15	02:00:00	18176	$9.61 \pm 0.06$
3C 445	1988-Nov-02	06:40:00	1988-Nov-03	07:00:00	27648	$6.92 \pm 0.05$

**Table 3.** The observation log for *ASCA*. The count rates for SIS and GIS are given in the 0.55–10 keV energy band. The statistical errors of the count rates are  $< 0.01 \text{ s}^{-1}$ , except for 3C 445, where the error is  $< 0.002 \text{ s}^{-1}$ .

Object	Date	Start time	Exposure [s]				Count rate [ $\text{s}^{-1}$ ]			
			SIS0	SIS1	GIS2	GIS3	SIS0	SIS1	GIS2	GIS3
3C 111	1996-Feb-13	12:35:19	10200	32100	35400	35400	0.62	0.48	0.50	0.62
3C 120	1994-Feb-17	15:42:24	43500	43100	42100	42100	1.67	1.32	0.98	1.23
3C 382	1994-Apr-18	09:24:22	18300	18000	35100	32700	1.50	1.00	1.10	0.84
3C 390.3	1993-Nov-16	22:40:14	28800	31000	42400	42400	0.49	0.40	0.30	0.39
	1995-Jan-15	09:20:11	8500	8600	13800	13800	0.54	0.46	0.36	0.44
	1995-May-06	00:02:12	10800	10800	13000	13000	0.96	0.81	0.62	0.72
3C 445	1995-Jun-01	11:43:49	33600	34200	35300	35300	0.057	0.048	0.046	0.063

**Table 4.** The observation log for OSSE. VP stands for the Viewing Period of *CGRO*. The net exposure time and the count rates are normalized to a single OSSE detector. The count rates and the photon fluxes (in units of  $10^{-4} \text{ s}^{-1} \text{ cm}^{-2}$ ) are given for the 50–150 keV band, and the energy spectral index,  $\alpha$ , for the 50–500 keV band.

Object	VP	Start date	End date	Exposure [s]	Count rate [ $10^{-2} \text{ s}^{-1}$ ]	Photon flux	$\alpha$
3C 111	4	1991-Jun-28	1991-Jul-12	440,233	$15.04 \pm 2.52$	$3.20 \pm 0.60$	$1.04 \pm 0.34$
	29	1992-May-14	1992-Jun-04	184,973	$5.64 \pm 3.67$	$1.86 \pm 1.12$	$-0.21 \pm 1.06$
	Sum	1991-Jun-28	1992-Jun-04	625,206	$12.26 \pm 2.08$	$2.81 \pm 0.54$	$1.00 \pm 0.35$
3C 120	29	1992-May-14	1992-Jun-04	162,711	$9.19 \pm 3.91$	$2.34 \pm 1.21$	$0.63 \pm 0.79$
	30	1992-Jun-04	1992-Jun-11	154,046	$< 9.22$	$< 2.21$	
	33	1992-Jul-02	1992-Jul-16	298,222	$19.75 \pm 3.30$	$4.60 \pm 0.78$	$2.02 \pm 0.50$
	220	1993-May-08	1993-May-13	94,259	$17.68 \pm 5.00$	$3.91 \pm 1.16$	$1.25 \pm 0.81$
	224	1993-Jun-04	1993-Jun-14	459,622	$15.12 \pm 2.23$	$3.41 \pm 0.52$	$1.20 \pm 0.34$
	317	1994-Feb-17	1994-Mar-01	208,365	$8.16 \pm 4.29$	$1.63 \pm 1.01$	$0.55 \pm 0.83$
	320	1994-Mar-08	1994-Mar-15	201,880	$8.11 \pm 4.53$	$2.05 \pm 1.07$	$4.10 \pm 2.28$
	617.1	1997-Mar-18	1997-Apr-01	669,576	$9.01 \pm 2.72$	$1.96 \pm 0.65$	$0.68 \pm 0.58$
	617.7	1997-Apr-07	1997-Apr-09	109,300	$13.77 \pm 7.38$	$3.28 \pm 1.76$	
	Sum	1992-May-14	1997-Apr-09	2,357,981	$11.22 \pm 1.25$	$2.54 \pm 0.30$	$1.10 \pm 0.26$
3C 390.3	12	1991-Oct-18	1991-Oct-31	375,313	$18.07 \pm 2.92$	$4.04 \pm 0.69$	$1.38 \pm 0.43$
	29	1992-May-15	1992-Jun-04	390,664	$11.55 \pm 2.52$	$2.58 \pm 0.60$	$1.19 \pm 0.45$
	209	1993-Feb-10	1993-Feb-22	330,724	$5.69 \pm 3.13$	$1.26 \pm 0.74$	$1.19 \pm 1.08$
	Sum	1991-Oct-18	1993-Feb-22	1,096,700	$12.01 \pm 1.64$	$2.54 \pm 0.40$	$1.36 \pm 0.32$
Sum		1991-Jun-28	1997-Apr-09	4,079,887	$11.34 \pm 0.91$	$2.57 \pm 0.22$	$1.15 \pm 0.16$

the “bright” mode for those 2 objects, see Sections 4.2 and 4.4.

The resulting spectra were then binned to assure that there are  $\geq 20$  counts per bin. In addition, for the observation of 3C 120, due to an on-board electronics malfunction in the GIS3 – where the two least significant bits of the analog-to-digital converter in the Pulse Height Discriminator circuit were stuck in a fixed pattern – all data for GIS3 needed to be binned with at least 8 channels to a bin. In all cases, the source photons were extracted using circular regions, with radii of  $3'$  for the SISs, and  $6'$  for the GISs, while the background, to be subtracted prior to the spectral fits from the source counts to get the net spectra, was extracted from suitable source-free regions of a size comparable or greater than the source regions.

For the GIS data, in our spectral fitting, we used the standard GIS response matrices (v4.0). For the SIS data, we used the SIS response matrix generator (SISRMG), as appropriate to every observation and detector, v1.1, April 1997. For both SIS and GIS data, we used the telescope effective areas (via the use of ASCAARF v2.72, March 1997). To account for the residual errors in the relative cross-calibration of the four telescopes, we fit the same model to the four data sets with each normalization as a free parameter. For plotting purpose only, we further rebin, renormalize and add the data from all 4 detectors using the normalization of SIS0. That normalization is also used for comparison with results of other instruments. We note that the relative normalization differences in our data with respect to SIS0 are  $< 13$  per cent except for the 3C382 observation (which used the non-standard observation configuration as described above) where the differences are  $< 26$  per cent.

Most of the OSSE data used here have been briefly reported in Johnson et al. (1997). The analysis of 3C 111 [2], 3C 120 [9] and 3C 390.3 [3] takes into account a systematic error correction to the spectra computed from the uncertainties in calibration and response of the detectors using both in-orbit and pre-launch data. The systematic errors correspond to  $\sim 3$  per cent uncertainty in effective area at 50 keV, decreasing to  $\sim 0.3$  per cent at 150 keV and above. We use the OSSE response matrix as revised in 1995, which results in the 50–60 keV fluxes about 20 per cent higher than in the original response (used, e.g., in Z95). Observation log for OSSE is given in Table 4.

We supplement the above data set by selected data from *EXOSAT*. We use *EXOSAT* ME spectra from the HEASARC archive with the quality flag 3 or higher, which indicates observations with reliable background subtraction (note that this criterion removes 3C 111 from the sample). The objects are 3C 120 [14], 3C 382 [24], 3C 390.3 [4], and 3C 445 [1] (some of those observations are reported in Turner & Pounds 1989). The usable *EXOSAT* energy range is from 1.2 keV to 8 keV in most cases as the spectra above 8 keV suffer from relatively inaccurate background subtraction. The individual spectra include a 1 per cent systematic error. Since the individual spectra are of rather low statistical significance, we use co-added spectra of each of the first 3 objects with the weights corresponding to the length of time of each observation. Both the counts and the response matrices for each observation were added using the ADDSPEC function of the FTOOLS data processing package. Time intervals covered by the observations are 1983 March–1986 Febru-

ary, 1983 September–1985 September, 1985 February–1986 March, and 1984 May for 3C 120, 3C 382, 3C 390.3 and 3C 445, respectively. We note that the Fe K line energies in the *EXOSAT* data appear at energies significantly lower than those obtained with *Ginga* and *ASCA*, which appears to be due to a calibration problem.

### 3 SPECTRAL MODELS

We use XSPEC (Arnaud 1996) v9 and 10 for spectral fitting. The parameter uncertainties in Tables below correspond to 90 per cent confidence for a single parameter, i.e.,  $\Delta\chi^2 = +2.7$ . On the other hand, the plotted error bars are  $1\text{-}\sigma$ , the upper limits,  $2\text{-}\sigma$ , and the spectral data are rebinned for clarity of display.

Fitted intrinsic spectra are absorbed by intervening matter with the column density that consists of both the Galactic component,  $N_{\text{H,G}}$  (see Table 1), and the column density intrinsic to the source,  $N_{\text{H}}$  (note that  $N_{\text{H}}$  does not include  $N_{\text{H,G}}$ ). Both the intrinsic spectra and absorption by  $N_{\text{H}}$  are evaluated at the source redshift,  $z$ . The absorption is in neutral matter with the abundances of Anders & Ebihara (1982) and the opacities of Morrison & McCammon (1983), as implemented in the **zwabs** model of XSPEC.

We model the underlying continuum as a power law with an energy spectral index,  $\alpha$ , multiplied by an exponential with an e-folding energy,  $E_c$ . When fitting the X-ray data only, we assume  $E_c = 400$  keV, consistent with results of Z95. This, however, has a negligible effect on the resulting parameters. On the other hand,  $E_c$  is a free parameter in fits to combined X $\gamma$  data.

We also allow for the presence of a Compton-reflection spectral component (Lightman & White 1988). Compton reflection arises when the underlying component irradiates cold matter in the vicinity of the nucleus, e.g., an accretion disk or a torus. We use Green’s functions for angle-dependent reflection of isotropic incident radiation of Magdziarz & Zdziarski (1995), and assume the viewing angle of  $30^\circ$  (corresponding to an orientation close to face-on, as expected in type-1 AGNs, Antonucci 1993, see also Eracleous, Halpern & Livio 1996 for 3C 390.3). The relative amount of reflection is measured by the solid angle subtended by the reflector,  $\Omega$  ( $\Omega = 2\pi$  corresponds to reflection from an infinite slab). The opacities of reflector are the same as for the absorber. However, we consider some models with the Fe abundance with respect to that of Anders & Ebihara (1982),  $A_{\text{Fe}}$ , being  $> 1$ . In some cases, we also allow the reflecting medium to be ionized, in which case we use the model of Done et al. (1992) modified as in Gondek et al. (1996). We assume the reflector temperature of  $10^5$  K (Krolik & Kallman 1984). The ionization parameter is defined as  $\xi \equiv L_{\text{ion}}/nr^2$ , where  $L_{\text{ion}}$  is the luminosity in an incident power-law continuum in the 5 eV–20 keV range,  $n$  is the density, and  $r$  the distance between the source of radiation and the reflector. The neutral and ionized reflection is implemented in the XSPEC models **pextrav** and **pextriv**, respectively.

Both reflection and absorption of the continuum are accompanied by emission of fluorescent lines, the most prominent of those is the Fe K $\alpha$  line (at 6.4 keV in the case of neutral Fe), which we model as a Gaussian at an energy,

$E_{\text{Fe}}$ , with a width,  $\sigma_{\text{Fe}}$ , and a photon flux,  $I_{\text{Fe}}$ . The line equivalent width is denoted by  $W_{\text{Fe}}$ . The line flux is allowed to be a free parameter, independent of both the amount of reflection and absorption (unless stated otherwise in the text). In fitting the data from *Ginga* and *EXOSAT*, we assume the fixed  $\sigma_{\text{Fe}} = 0.1$  keV. On the other hand,  $\sigma_{\text{Fe}}$  is a free parameter in fits to the *ASCA* data, which have energy resolution much better than those of *Ginga* and *EXOSAT*. In fits to *ASCA* data, we include, in addition to the  $K\alpha$  line, the Fe  $K\beta$  and Ni  $K\alpha$  lines, a sum of which we model as a single line with the energy, width, and normalization equal 1.1, 1.1, and 0.2, respectively, of the corresponding values for Fe  $K\alpha$  (e.g., Życki & Czerny 1994). For simplicity, we denote below both lines as Fe K. The line parameters given below for *ASCA* data correspond to the Fe  $K\alpha$  component only. (Note that for clarity of plotting *ASCA* data, we use  $\sigma_{\text{Fe}} = 0.1$  keV whenever fitting yields a lower value.) Except for 3C 445 and Cen A, we assume the lines are absorbed in the same way as the continuum.

## 4 RESULTS OF SPECTRAL FITS

### 4.1 3C 445

3C 445 is a powerful FR II BLRG with a typical lobe-dominated radio morphology and an elliptical appearance in the optical band (Smith & Heckman 1989). The source lies  $\sim 0.5^\circ$  from the cluster A 2440, which thus contaminates the spectrum of 3C 445 (Pounds 1990) from *Ginga* (which has the field of view of  $1^\circ \times 2^\circ$ ). The cluster emission has been modelled by Pounds (1990) as thermal bremsstrahlung at  $kT = 3$  keV. We note that component would also include any soft X-ray excess of the AGN itself. We fit the updated *Ginga* data (see Section 2) by the sum of that component, an absorbed power law with Compton reflection and an Fe K line, and obtain the parameters given in the Table 5. They are consistent with those of Pounds (1990) within the statistical uncertainties, although Pounds (1990) obtains a somewhat softer spectral index,  $\alpha = 0.68^{+0.20}_{-0.18}$ , which is apparently due to differences in data processing. Similarly to Pounds (1990), we find the X-ray source is strongly obscured. The *Ginga* spectrum is shown in Figure 1a.

We see in Table 5 that the *Ginga* data do not require the presence of a Compton reflection component, and  $\Omega/2\pi \lesssim 0.2$ . (The top-layer *Ginga* data alone are consistent with this result, but yield a weaker constraint of  $\Omega/2\pi = 0.20^{+0.64}_{-0.20}$ .) On the other hand, there is a strong Fe K line in the spectrum (modeled here as absorbed by  $N_{\text{H,G}}$  only). The line originates in both the cluster and the AGN. The cluster emits a thermal emission line at the rest-frame energy of 6.7 keV with  $W_{\text{Fe}} \simeq 500$  eV with respect to the bremsstrahlung spectrum (Pounds 1990 and references therein). At  $z = 0.094$  of A 2440 (Struble & Rood 1987), the observed centroid energy of the cluster line is 6.12 keV and cannot be resolved by *Ginga* from the fluorescent line from 3C 445 redshifted from 6.4 keV to 6.05 keV. Thus, we model both line components as a single Gaussian. The line flux,  $I_{\text{Fe}}$ , in Table 5 corresponds to both components, whereas the stated  $W_{\text{Fe}}$  corresponds to the AGN component only with respect to the absorbed power-law continuum.

The *ASCA* data, on the other hand, are basically free

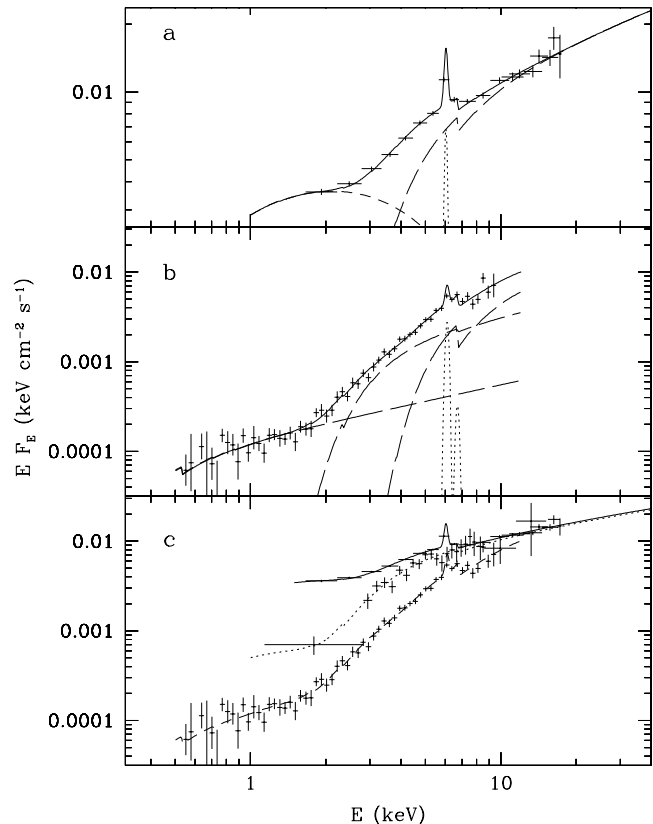


**Figure 1.** The X-ray spectra (crosses) of 3C 445. (a) The data from *Ginga*, with emission from the nearby cluster A 2440 modeled as bremsstrahlung (short dashes), an absorbed power-law emission of 3C 445 (long dashes), and an Fe K line emission (dots) from both the AGN and the cluster. The solid curve is the sum. (b) The data from *ASCA* (which contain no contribution from the cluster). The spectrum is modeled as the sum (solid curve) of 3 power-law components (long dashes) with the same  $\alpha$  but different  $N_{\text{H}}$ , and an Fe K line (dots). (c) Comparison of the spectra from *Ginga*, *EXOSAT*, and *ASCA* (from top to bottom).

from contamination from the cluster. In our modeling of the continuum, we use a model with 3 power-law components each absorbed by a different column density, which was shown to be the simplest model accounting for the shape of the spectrum from *ASCA* in an early analysis of the data by Yamashita & Inoue (1996). The fit parameters are given in Table 5, and the spectrum is shown in Figure 1b. We see that the spectrum of 3C 445 contains a substantial soft X-ray excess component, modeled here as the third power-law component with  $N_{\text{H}}$  consistent with null (Table 5). That component can be interpreted as due to scattering of about 5 per cent of the intrinsic emission by a hot plasma in the funnel of an obscuring torus (Krolik & Kallman 1987). Then the remaining two absorbed power-law components can be interpreted as being due to the product of uniform absorption with  $N_{\text{H},2}$  and partial covering by  $(N_{\text{H},1} - N_{\text{H},2})$  with a covering fraction of  $A_1/(A_1 + A_2)$ .

The obtained spectral index and the line parameters are similar to those derived above from the *Ginga* data. In particular, the obtained line equivalent width is almost the same as  $W_{\text{Fe}}$  estimated above after subtracting the cluster component in the *Ginga* data. We also find the Fe K line

**Table 5.** Results of fits to the 3C 445 data from *Ginga*, *ASCA* and *EXOSAT*. The *Ginga* and *EXOSAT* data contain a cluster contribution at low energies, which is modeled by a 3-keV bremsstrahlung photon spectrum,  $A_2 \exp(-E/kT)$  times the Gaunt factor.  $A_1$  gives the 1-keV normalization of the power-law component. The *ASCA* continuum is modeled as the sum of 3 power-law components with the same  $\alpha$  but different normalizations,  $A_i$ , and columns,  $N_{H,i}$ . Hereafter, the normalizations are given in units of  $10^{-3} \text{ s}^{-1} \text{ cm}^{-2}$ ,  $N_H$  is given in  $10^{21} \text{ cm}^{-2}$ ,  $E_{\text{Fe}}$  and  $\sigma_{\text{Fe}}$  in keV,  $I_{\text{Fe}}$  in  $10^{-5} \text{ s}^{-1} \text{ cm}^{-2}$ ,  $W_{\text{Fe}}$  in eV, and ‘f’ denotes a fixed parameter.

$A_i$	$N_{H,i}$	$\alpha$	$\Omega/2\pi$	$E_{\text{Fe}}$	$\sigma_{\text{Fe}}$	$I_{\text{Fe}}$	$W_{\text{Fe}}$	$\chi^2/\text{dof}(\chi^2_\nu)$
$3.2^{+1.7}_{-0.6}, 4.3^{+0.2}_{-0.2}$	$150^{+30}_{-30}$ , Of	$0.45^{+0.14}_{-0.10}$	$0^{+0.22}$	$6.37^{+0.22}_{-0.19}$	0.1f	$4.7^{+1.7}_{-2.1}$	150	35.3/36(0.98)
$1.9^{+2.6}_{-1.2}, 0.87^{+0.54}_{-0.39}, 0.15^{+0.02}_{-0.02}$	$580^{+370}_{-230}, 78^{+21}_{-20}, 0^{+0.60}$	$0.39^{+0.28}_{-0.29}$	Of	$6.44^{+0.07}_{-0.07}$	$0^{+0.18}$	$1.8^{+0.6}_{-0.7}$	140	429/421(1.02)
$2.5^{+9.0}_{-1.4}, 0.62^{+0.87}_{-0.62}$	$80^{+100}_{-50}$ , Of	$0.33^{+0.77}_{-0.40}$	Of	–	–	Of	–	35.8/43(0.83)

is narrow,  $\sigma_{\text{Fe}} < 0.18$  keV. The  $\sigma_{\text{Fe}}-E_{\text{Fe}}$  confidence contours are presented in Figure 2, and the line profile is shown in Figure 3. Note that the presence of a soft excess component in the spectrum of 3C 445 shown by *ASCA* implies that a (minor) part of the soft excess (modeled as bremsstrahlung) in the *Ginga* and *EXOSAT* data actually comes from the AGN itself.

Our *ASCA* results can be compared with a recent independent analysis of the data by Sambruna et al. (1998). Their best-fit model has the identical form to ours. However, they obtain a harder power law than that obtained by us, with  $\alpha = 0.25^{+0.29}_{-0.27}$ , and a broader and stronger Fe K line, with  $\sigma_{\text{Fe}} = 0.16^{+0.16}_{-0.13}$  keV (in the source frame), and  $I_{\text{Fe}} = (5.0^{+4.0}_{-2.5}) \times 10^{-5} \text{ s}^{-1} \text{ cm}^{-2}$ . These differences can be explained by their use of an earlier (of 1994) version of the *ASCA* software than that used by us (of 1997). Furthermore, the reduced  $\chi^2$  of their best-fit model is statistically significantly larger than ours (1.05 vs. 1.02). Thus, we conclude that the *ASCA* data are fully compatible with the Fe K line being narrow, as obtained by us.

The  $W_{\text{Fe}} \sim 150$  eV obtained by us for both *Ginga* and *ASCA* data is consistent with emission of a shell of cold matter with  $N_H \sim (2-5) \times 10^{23} \text{ cm}^{-2}$  and the cosmic Fe abundance irradiated isotropically from the center (Makishima 1986, hereafter M86; Awaki et al. 1991). We thus conclude that the most likely origin of the Fe K emission in 3C 445 is fluorescence in the observed absorber, which, we infer, covers a large solid angle around the nucleus. This interpretation is consistent with the narrowness of the line derived from the *ASCA* data. The presence of an optically-thick disk irradiated isotropically by the X-ray source appears to be ruled out as the solid angle of any reflector is constrained to  $\ll 2\pi$ .

Figure 1c shows a comparison of 3C 445 spectra from different instruments. Here, we also show the spectrum from *EXOSAT*, fitted in the 1–15 keV range in the same way as the *Ginga* data except that the Fe K line is not included in the model due to the limited statistical quality of the former data. The cluster contribution to the *EXOSAT* data is about a quarter of that in the *Ginga* data, which is fully consistent with the field of view of *EXOSAT* ( $45' \times 45'$ ) being smaller than that of *Ginga*. On the other hand, the spectra of the AGN itself from *Ginga* and *EXOSAT* are consistent with being the same. However, the *ASCA* spectrum lies significantly below the other two spectra even at hard X-ray energies, where the cluster contribution is negligible. This indicates the presence of X-ray variability in 3C 445, caused

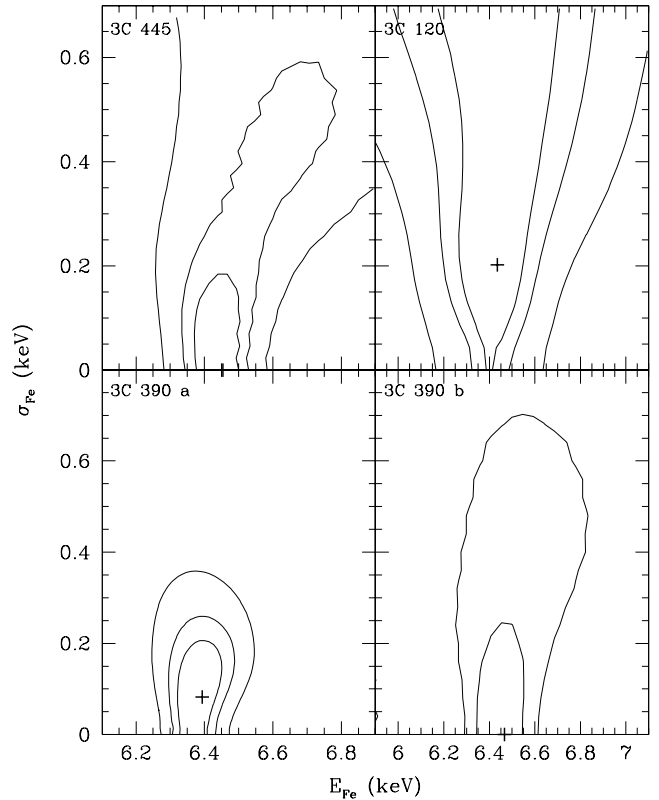


**Figure 2.** The confidence contours (at 68, 90, and 99 per cent) for the energy and the width of the iron line (in the source frame) for the *ASCA* observations showing statistically significant lines. Models with Compton reflection are used except for 3C 445, see Tables 5, 7, 9.

by either variability of the power-law component or variable absorption.

## 4.2 3C 111

3C 111 is a luminous FR II radio galaxy with bright core, a one-sided jet on milli-arcsecond scale (Linfield & Perley 1984), a highly asymmetric double radio structure, and reported superluminal motion ( $\gtrsim 10c$ , Preuss, Alef & Kellermann 1988). The optical image shows no structure (Colina & Pérez-Fournon 1990) and thus exact classification is not

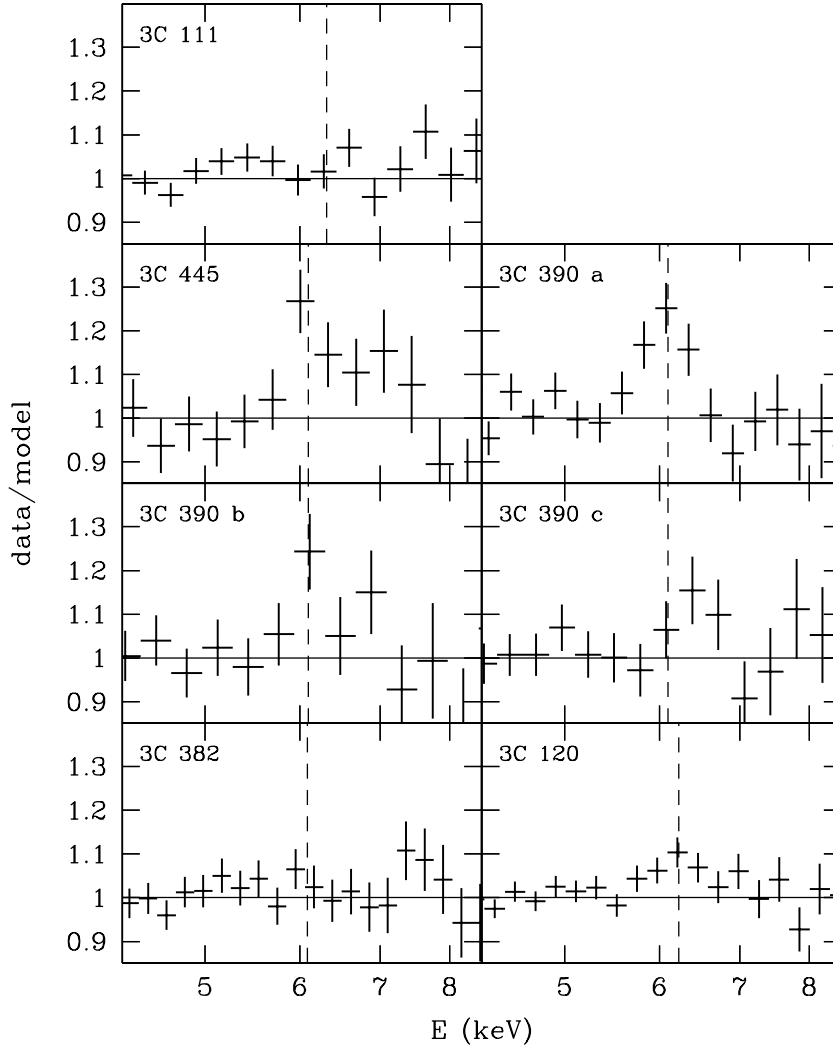


**Figure 3.** The line profiles for all presented *ASCA* observations, modeled including Compton reflection except for 3C 445, see Tables 5-9. The data have been fitted including the Fe K line, which then was removed from the model in the displayed ratios. The vertical dashed lines correspond to 6.4 keV at the redshift of each source.

**Table 6.** Results of fits to the *Ginga* and *ASCA* spectra of 3C 111.

$A$	$\alpha$	$N_{\text{H}}$	$\Omega/2\pi$	$E_{\text{Fe}}$	$\sigma_{\text{Fe}}$	$I_{\text{Fe}}$	$W_{\text{Fe}}$	$\chi^2/\text{dof}(\chi^2_{\nu})$
<i>Ginga</i> 1989 Feb								
$10.5^{+0.14}_{-0.09}$	$0.82^{+0.08}_{-0.06}$	$18^{+2}_{-2}$	$0.12^{+0.31}_{-0.12}$	$6.72^{+0.36}_{-0.32}$	0.1f	$2.7^{+1.7}_{-1.5}$	78	36.8/34(1.08)
$I_{\text{Fe}}/\Omega = \text{const}$								
11.3	$0.86^{+0.06}_{-0.07}$	$19^{+2}_{-2}$	$0.30^{+0.23}_{-0.21}$	$6.79^{+0.51}_{-0.46}$	0.1f	$2.0^{+1.5}_{-1.4}$	55	39/35(1.10)
<i>ASCA</i> 1996 Feb								
$9.6^{+0.4}_{-0.3}$	$0.73^{+0.03}_{-0.02}$	$7.3^{+0.3}_{-0.3}$	0.12f	$6.78^{+\infty}_{-6.78}$	0.1f	$1.0^{+1.4}_{-1.0}$	25	1418/1511(0.94)

possible, but the properties of the host galaxy are consistent with elliptical morphology.

The spectrum of 3C 111 from *Ginga* was included in the sample of NP94. The parameters of our fits to the *Ginga* observation are reported in Table 6 and the spectrum is shown in Figure 4. The Fe K line energy,  $\sim 6.7$  keV (although lower than 7.4 keV found by NP94), suggests emission by strongly ionized iron. The remaining fit parameters are sim-

ilar to those of NP94, in particular there is little evidence for reflection. (The top-layer *Ginga* data alone are also consistent with the absence or weakness of reflection, yielding  $\Omega/2\pi = 0^{+0.16}$ .) On the other hand, the best-fit value of  $W_{\text{Fe}} \simeq 80$  eV appears too large for the Fe K line to be due to reflection. However, the uncertainties on the fitted parameters are such that the origin of the Fe K line from Compton reflection is still possible. In particular, we have

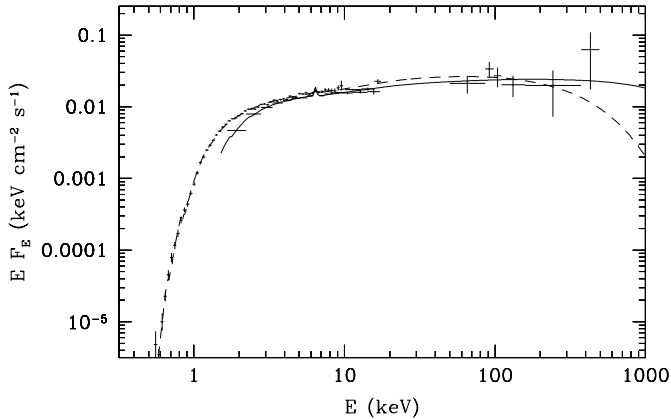


**Figure 4.** The spectrum of 3C 111 from the 1989 observation by *Ginga* (the bottom X-ray spectrum), the 1996 observation by *ASCA* (the top X-ray spectrum), and the 1991-92 OSSE spectrum ( $> 50$  keV).

fitted a model in which the line equivalent width was tied to the reflected component. Theoretical estimates of  $W_{\text{Fe}}$  with respect to the Compton-reflected component are relatively uncertain and vary from  $\sim 0.7$  keV to  $\sim 1.5$  keV for  $\Omega = 2\pi$ ,  $\alpha = 0.9$  and  $A_{\text{Fe}} = 1$  (Życki & Czerny 1994; George & Fabian 1991; hereafter GF91). The line becomes stronger with increasing Fe abundance (GF91). Here, we adopt the highest value of 1.5 keV for  $A_{\text{Fe}} = 1$  and increase it with increasing  $A_{\text{Fe}}$  according to the results of GF91. We find that already for  $A_{\text{Fe}} = 1$ ,  $\Omega/2\pi \sim 0.3$  at  $\Delta\chi^2 \simeq +2$  (Table 6) which increase is not significant statistically. This means that the line emission from 3C 111 can originate from Compton reflection, but the  $\Omega/2\pi \sim 0.3$  implies the reflector geometry is different from a slab.

We have tested whether ionization of the reflector can relax the constraints on the solid angle obtained above. We have found that the *Ginga* data cannot constrain the ionization parameter at all, but the best-fit  $\xi = 0$ . When we fix  $\xi$  at a large value, e.g.,  $\xi = 5000$  erg s $^{-1}$  cm $^{-1}$ , the allowed solid angle of the reflector *decreases* with respect to neutral reflection:  $\Omega/2\pi = 0^{+0.09}$ . This decrease is a consequence of a larger depth of the K edge from an ionized medium than a neutral one with the data consistent with no K edge. Thus, the small values of  $\Omega/2\pi$  obtained here are not an artefact of the assumption of the neutrality of the reflector. On the other hand, the reflected X-ray spectrum would have the same shape as the incident spectrum in the limit of complete ionization of all elements in the reflector (White, Lightman & Zdziarski 1988), which would then allow any value of  $\Omega$ , in particular  $2\pi$ . However, such strong ionization would lead to *no* Fe K  $\alpha$  line.

In fitting the *ASCA* data, we assumed the best-fit  $\Omega/2\pi$  obtained from the *Ginga* data, which, due to the weakness of Compton reflection, affects little the fit. We find only a weak Fe K line in these data, with  $W_{\text{Fe}} \sim 25^{+30}_{-25}$  eV, see Table 6 and Figure 3. Due to its weakness, the line parameters are not constrained, and  $\sigma_{\text{Fe}}$  has been fixed at 0.1 keV while determining the confidence contours of other parameters.

We have investigated whether we could somehow miss a broad and strong Fe K line still present in the *ASCA* spec-

trum. First, we have found that the line disappears altogether from the model if Compton reflection is assumed to be strong,  $\Omega/2\pi = 1$ , which  $\Omega$  is expected in the case of line formation in an inner region of an accretion disk. Second, we have considered the effect of using the SIS0 data obtained in the bright mode, which increases the exposure available for that detector by a factor of about 2.5 (but degrades the energy resolution, see Section 2). We find that then the Fe K line in the combined SIS/GIS data becomes only slightly stronger, with the best-fit  $W_{\text{Fe}} \simeq 35$  eV. Again, the assumption of  $\Omega/2\pi = 1$  results in disappearing of the line. If the SIS0 and SIS1 data are used without the GIS data (which have a worse energy resolution),  $\sigma_{\text{Fe}} \simeq 0.2^{+1.1}_{-0.2}$  keV, and the best-fit  $W_{\text{Fe}} \simeq 60$ –90 eV are obtained for  $\Omega/2\pi$  between 1 and 0.12. Thus, any Fe K line in the data is at most moderate and its strong broadening is neither required nor implied by the data.

The *ASCA* data show little intrinsic spectral variability with respect to the *Ginga* data, see Table 6 and Figure 4. However, the *ASCA* data show a marked decrease of the absorbing column with respect to that seen by *Ginga*. This decrease correlates with the apparent decrease of the Fe K line flux between the *Ginga* and *ASCA* observations, which suggests the origin of the line primarily in the absorber. Although the best-fit value of  $W_{\text{Fe}}$  from *Ginga* is a factor of  $\sim 3$  larger than that expected from a shell of absorbing, isotropically-irradiated, matter with the best-fit value of  $N_{\text{H}}$  (M86), the uncertainties on the line flux and on the reflector solid angle are such that comparable parts of the line can come from the absorber and the reflector. In that case a decrease of  $N_{\text{H}}$  would lead to a noticeable decrease of  $I_{\text{Fe}}$ , explaining the weakness of the Fe K line in the *ASCA* data.

Figure 4 also shows the 1991–92 spectrum from OSSE. The OSSE spectrum, although not simultaneous with other observations presented here, is consistent with extrapolation of both the *Ginga* and *ASCA* power laws. Some spectral steepening at high energies is, however, possible. Fits to the combined *Ginga*/OSSE and *ASCA*/OSSE data yield  $E_c = 1.6^{+0}_{-1.3}$  MeV and  $300^{+460}_{-130}$  keV, respectively. The models corresponding to the best-fit values of  $E_c$  are plotted in Figure 4.

### 4.3 3C 390.3

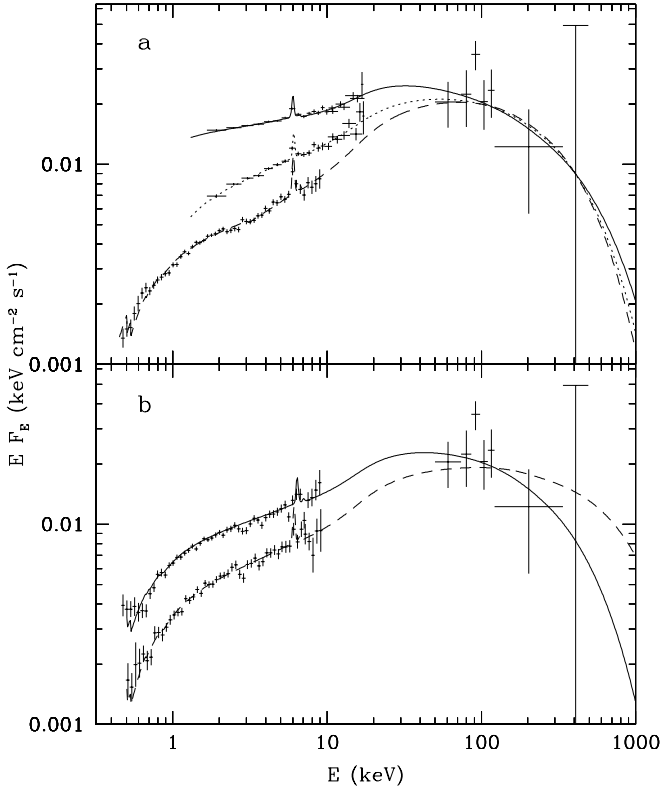
The optical morphology of this powerful radio galaxy is unusual; there are no spiral arms, but the luminosity profile does not follow the  $r^{1/4}$  law in the outer parts of the image (Smith & Heckman 1989). In the radio frequencies, the object is lobe-dominated and displays superluminal motion (Wamsteker & Clavel 1989 and references therein). The galaxy has been observed by *EXOSAT*, *Ginga*, *ASCA*, and OSSE.

We first analyze the spectra from *Ginga*, shown in Figure 5a. Our 1991 data exclude a period when a stellar flare occurred in the field of view of *Ginga* (Inda et al. 1994). The 1988 observation has been included in the NP94 sample, and the 1991 observation has been presented by Inda et al. (1994), who, however, have not searched for the presence of Compton reflection. We note a possible presence of a soft-excess component in the 1988 data, as indicated by the null value of the best-fit  $N_{\text{H}}$  and positive residuals seen in the lowest *Ginga* channels (see Fig. 3 of Inda et al. 1994).



**Table 7.** Results of fits to the *Ginga*, *ASCA* and *EXOSAT* spectra of 3C 390.3. The fit to the 1993 November *ASCA* data set with Compton reflection is limited to the 3–10 keV energy range.

$A$	$\alpha_s$	$N_H$	$E_b$	$\alpha$	$\Omega/2\pi$	$E_{Fe}$	$\sigma_{Fe}$	$I_{Fe}$	$W_{Fe}$	$\chi^2/\text{dof}(\chi^2_\nu)$
<i>Ginga</i> 1988 Nov										
$13.3^{+0.2}_{-0.2}$	–	$0.0^{+0.2}$	–	$0.84^{+0.01}_{-0.01}$	0f	$6.33^{+0.31}_{-0.30}$	0.1f	$2.8^{+1.4}_{-1.4}$	58	43.8/35(1.25)
$14.0^{+0.5}_{-0.4}$	–	$0.0^{+0.5}$	–	$0.90^{+0.03}_{-0.03}$	$0.35^{+0.15}_{-0.24}$	$6.33^{+0.27}_{-0.27}$	0.1f	$3.4^{+1.3}_{-1.3}$	67	28.1/34(0.83)
<i>Ginga</i> 1991 Feb										
$5.7^{+0.4}_{-0.2}$	–	$0.2^{+1.6}_{-0.2}$	–	$0.64^{+0.04}_{-0.03}$	0f	$6.36^{+0.41}_{-0.44}$	0.1f	$2.5^{+1.4}_{-1.5}$	84	31.2/35(0.89)
$6.2^{+0.3}_{-0.7}$	–	$1.6^{+2.3}_{-1.6}$	–	$0.70^{+0.03}_{-0.08}$	$0.26^{+0.37}_{-0.26}$	$6.41^{+0.42}_{-0.46}$	0.1f	$2.7^{+1.4}_{-1.3}$	86	29.0/34(0.85)
<i>ASCA</i> 1993 Nov										
$3.8^{+0.1}_{-0.1}$	–	$0.4^{+0.1}_{-0.1}$	–	$0.68^{+0.01}_{-0.03}$	0f	$6.40^{+0.08}_{-0.07}$	$0.20^{+0.12}_{-0.13}$	$4.6^{+1.0}_{-1.4}$	240	1326/1314(1.01)
$3.9^{+0.1}_{-0.1}$	$0.74^{+0.04}_{-0.04}$	$0.5^{+0.1}_{-0.5}$	$3.3^{+0.4}_{-0.5}$	$0.54^{+0.05}_{-0.05}$	0f	$6.38^{+0.07}_{-0.06}$	$0.10^{+0.12}_{-0.10}$	$3.2^{+1.1}_{-1.1}$	150	1309/1312(1.00)
$3.1^{+0.2}_{-0.1}$	–	0.5f	–	$0.56^{+0.07}_{-0.06}$	0.35f	$6.38^{+0.08}_{-0.06}$	$0.08^{+0.13}_{-0.08}$	$2.9^{+1.2}_{-1.0}$	140	545/587(0.93)
<i>ASCA</i> 1995 Jan										
$4.5^{+0.2}_{-0.2}$	–	$0.8^{+0.2}_{-0.2}$	–	$0.70^{+0.04}_{-0.03}$	0.35f	$6.44^{+0.11}_{-0.11}$	$0.00^{+0.33}$	$2.8^{+1.6}_{-1.4}$	120	646/743(0.87)
<i>ASCA</i> 1995 May										
$7.8^{+0.4}_{-0.1}$	–	$0.4^{+0.2}_{-0.1}$	–	$0.77^{+0.03}_{-0.03}$	0.35f	$6.75^{+0.39}_{-0.43}$	$0.20^{+\infty}_{-0.20}$	$2.3^{+3.1}_{-1.8}$	84	1048/1017(1.03)
<i>EXOSAT</i> 1985–86										
5.3	–	$0.0^{+4.1}$	–	$0.61^{+0.16}_{-0.07}$	0.3f	$5.91^{+\infty}_{-5.91}$	0.1f	$1.1^{+5.5}_{-1.1}$	32	20/22(0.90)


**Figure 5.** X-ray spectra of 3C 390.3. (a) The *Ginga* spectra from 1988 and 1991, and the *ASCA* spectrum from 1993, from top to bottom, respectively. (b) The *ASCA* spectra from 1995 May (top) and January (bottom). Above 50 keV, the average spectrum from 1991–93 observations by OSSE is shown on both panels. The model curves include reflection and high-energy cutoffs implied by the OSSE data.

We find a moderate Compton reflection component corresponding to  $\Omega/2\pi \sim 0.3$  in both observations (Table 7), which is similar to the result of NP94 for the 1988 observation. The presence of reflection is significant in the (longer)

1988 observation at the 99.99 per cent confidence level. (The top-layer *Ginga* data alone imply somewhat stronger reflection, with  $\Omega/2\pi = 0.50^{+0.26}_{-0.20}$  in 1988 and  $0.51^{+0.74}_{-0.39}$  in 1991, which values are still consistent within statistical errors with those in Table 7.)

We have also considered the effect of the reflector ionization. Similarly to the case of 3C 111, we find that ionization of the reflector has a negligible effect on  $\Omega$ ;  $\xi = 0^{+122}$  erg  $\text{s}^{-1} \text{cm}^{-1}$ , and  $\Omega/2\pi = 0.33^{+0.18}_{-0.17}$  at the upper limit of  $\xi$  for the 1988 *Ginga* data. Similar results are obtained for the 1991 observation.

Results of *ASCA* observations of 3C 390.3 in 1993 and 1995 have been reported in Eracleous et al. (1996) and Leighly et al. (1997), respectively. Here, we reanalyse those data using the current version of the response and the effective area of *ASCA* (see Section 2). First, we fit the data from 1993 with a power-law continuum, a Gaussian line, and neutral absorption, see Table 7. Our results on both the continuum and the line are similar to those of Eracleous et al. (1996), in particular,  $\alpha \simeq 0.7$  and  $\sigma_{Fe} \simeq 0.2$  keV. However, the data show strong evidence for the presence of a soft excess, as demonstrated by a large reduction of  $\chi^2$  (by  $-17$  for addition of 2 parameters, which is significant at the 99.98 per cent confidence) when the power law is allowed to break. This is consistent with the possible presence of a soft X-ray excess in the 1988 *Ginga* data (see above) as well as in the *EXOSAT* data (Ghosh & Soundararajaperumal 1991). The broken power law model gives  $\alpha \simeq 0.5$ – $0.6$  above  $\sim 3$  keV, and the Fe line both weaker than for the single-power law fit as well as unresolved at the  $1$ - $\sigma$  level. The energy-width confidence contours and the line profile are shown in Figures 2 and 3, respectively.

As found above, the *Ginga* data above show the presence of Compton reflection. However, including it only weakly affects the results of the *ASCA* spectral fits, as shown in Table 7. The main effect is that the Fe K line becomes slightly weaker and narrower than in the case without Compton reflection. The *ASCA* spectrum modeled including Compton reflection is shown in Figure 5a.

Results similar to those discussed above are obtained

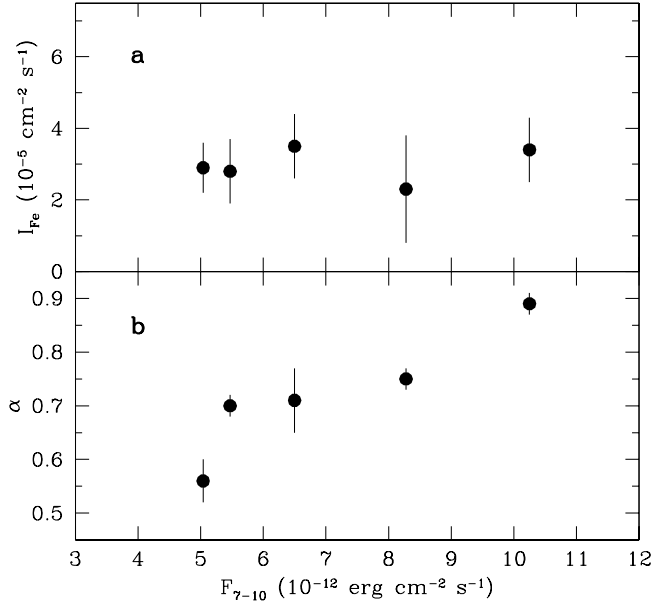


**Figure 6.** The dependences of (a) the flux of the Fe K line, and (b) the hard X-ray spectral index,  $\alpha$ , on the 7–10 keV continuum flux in 3C 390.3. The line flux is consistent with being independent of the continuum level whereas the continuum softens as the source brightens. The error bars are for the 1- $\sigma$  significance.

for the two *ASCA* observations of 1995. They are significantly shorter than that in 1993 (see Table 3), and thus constraints on the spectral parameters are weaker. We find those data do not require the presence of a spectral break in the continuum, i.e., the corresponding reductions in  $\chi^2$  are statistically insignificant. The Fe K line is unresolved at the 1- $\sigma$  level, see Table 7 and Figures 2 and 3. The 1995 *ASCA* spectra are shown in Figure 5b.

The fit results to the average 1985–86 *EXOSAT* spectrum are given in the last row of Table 7. We find this spectrum is very similar to that of the 1991 *Ginga* observation, therefore we omit it for clarity in Figure 5. Due to the limited usable energy range, it does not constrain the amplitude of the Compton reflection, and we give results  $\Omega/2\pi = 0.3$  only.

From Table 7, we see that the flux in the Fe line in all observations presented here is compatible with being constant,  $\sim 3 \times 10^{-5} \text{ cm}^{-2} \text{ s}^{-1}$ , whereas the Fe-K ionizing flux ( $\gtrsim 7 \text{ keV}$ ) varies by a factor of  $\sim 2$ , as illustrated in Figure 6a. The correlation coefficient between  $I_{\text{Fe}}$  and the 7–10 keV flux is  $r = 0.16$ , which corresponds to the probability that there is indeed no correlation between those quantities of  $> 45$  per cent. This argues against the bulk of the line being due Compton reflection from an inner region of an accretion disk, in which case a proportionality of the line to the flux would be expected. Furthermore,  $W_{\text{Fe}} \sim 100\text{--}150 \text{ eV}$  in the observations in 1993 and 1995 January cannot be accounted for by Compton reflection with  $\Omega/2\pi \sim 0.3$  (e.g., GF91), seen in both *Ginga* observations. (Eracleous et al. 1996 claimed the Fe K line in the 1993 observation could be entirely due to Compton reflection without considering its strength measured by *Ginga*.) On the other hand, the absorbing column is so low that it can account for at most

$W_{\text{Fe}} \sim 10 \text{ eV}$  (M86). Possible resolutions of this issue are discussed in Section 7 below.

Figure 6b shows that the X-ray spectrum softens when it brightens, as previously noted by Inda et al. (1994) and Leighly et al. (1997). This spectral variability yields spectra pivoting around 100 keV at a flux corresponding to the average 1991–93 OSSE data, see Figure 5. The OSSE data at higher energies lie below the extrapolation of the X-ray power laws, which implies the presence of a high-energy cutoff or break. E.g., the 1988 *Ginga* data imply  $E_c = 400^{+580}_{-170} \text{ keV}$  and the 1993 *ASCA* data yield  $E_c = 260^{+320}_{-110} \text{ keV}$ . Models with the high-energy cutoffs are plotted in Figure 5.

#### 4.4 3C 382

The radio morphology of 3C 382 is typical for two-lobe sources with characteristic hot spots (McDonald, Kenderdine & Neville 1968). Optically, it appears as a distorted elliptical (Smith & Heckman 1989) with extremely broad Balmer lines reaching  $\text{FWZI} \sim 25,000 \text{ km s}^{-1}$  (Osterbrock, Koski & Phillips 1975).

*Ginga* observed 3C 382 several times during 5 days in 1989 July (Kaastra, Kunieda & Awaki 1991). We have initially analyzed the *Ginga* spectra from the observation divided into 3 periods (as in Table 2). They are well described by a hard power-law spectrum with  $\alpha \simeq 0.5$  with neither intrinsic absorption nor Compton reflection and are almost identical. Therefore, we consider hereafter only the total spectrum. Table 8 gives the fit results, and Figure 7 shows the unfolded spectrum and the best-fit model. We see that allowing for the presence of Compton reflection does not improve the fit, and  $\Omega/2\pi \lesssim 0.3$ . (With the top-layer data only, a weaker constraint is obtained,  $\Omega = 0.22^{+0.53}_{-0.22}$ .) This differs from the corresponding fit in NP94, who obtained  $\Omega/2\pi \gtrsim 1$ . However, the reflection model of NP94 includes the Fe K $\alpha$  line tied to the reflection continuum (as in our models below) and the strong reflection in their fits is driven by the large flux in the line. Similarly as for 3C 111 and 3C 390.3, ionization of the reflector leads to a reduction of the fitted reflection strength; for a large  $\xi = 5000 \text{ erg s}^{-1} \text{ cm}^{-1}$ ,  $\Omega/2\pi = 0^{+0.15}$ .

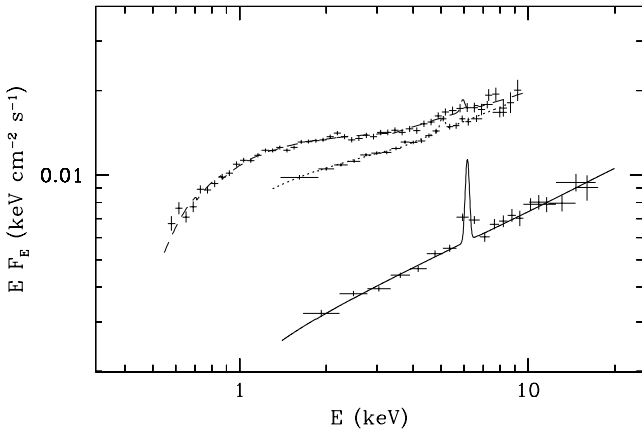
On the other hand, there is a pronounced Fe K line with  $W_{\text{Fe}} \simeq 220 \text{ eV}$  in the data. We find that this line is too strong to be explained by Compton reflection. Namely, when we tie the strength of the Fe line to the solid angle of the reflector (as in Section 4.2), the fit becomes significantly worse than in the case of the free line flux, even for the Fe abundance 4 times the solar value (Table 8).

Kaastra et al. (1991) have found the presence of a soft excess in the *Ginga* spectrum. We also see a similar component in our data. However, our analysis is constrained to the range  $\geq 1.7 \text{ keV}$  whereas Kaastra et al. also included the 1.2–1.7 keV *Ginga* channel (which calibration is in general less certain for weak sources). Thus, we do not attempt to constrain the form of the excess with the *Ginga* data.

A soft excess is seen very pronouncedly in the *EXOSAT* data (Ghosh & Soundararajaperumal 1992), which we also find in the average *EXOSAT* data, see Table 8 and Figure 7. Namely, the fit improves with  $\Delta\chi^2 = -11$  (corresponding to the statistical significance of 99 per cent) when a break in the power law spectrum is allowed. The continuum slope

**Table 8.** Results of fits to the *Ginga*, *EXOSAT* and *ASCA* spectra of 3C 382. The second fit with  $I_{\text{Fe}}/\Omega = \text{const}$  is for  $A_{\text{Fe}} = 4$ .

$A$	$\alpha_s$	$N_{\text{H}}$	$E_{\text{b}}$	$\alpha$	$\Omega/2\pi$	$E_{\text{Fe}}$	$\sigma_{\text{Fe}}$	$I_{\text{Fe}}$	$W_{\text{Fe}}$	$\chi^2/\text{dof}(\chi^2_{\nu})$
<i>Ginga</i> 1989 Jul										
$2.4^{+0.1}_{-0.1}$	–	$0.0^{+1.4}$	–	$0.50^{+0.06}_{-0.04}$	$0.05^{+0.28}_{-0.05}$	$6.52^{+0.20}_{-0.20}$	0.1f	$3.7^{+1.1}_{-1.2}$	220	29.6/34(0.87)
$I_{\text{Fe}}/\Omega = \text{const}$										
3.0	–	$3.2^{+2.9}_{-2.6}$	–	$0.68^{+0.11}_{-0.11}$	$0.89^{+0.52}_{-0.89}$	$6.59^{+0.26}_{-0.26}$	0.1f	$2.5^{+1.5}_{-2.5}$	160	47/35(1.35)
2.5	–	$0.0^{+2.2}$	–	$0.55^{+0.05}_{-0.04}$	$0.75^{+0.25}_{-0.25}$	$6.57^{+0.24}_{-0.24}$	0.1f	$3.0^{+1.0}_{-1.0}$	190	35/35(0.99)
<i>EXOSAT</i> 1983–85										
9.6	–	$0.0^{+0.3}$	–	$0.69^{+0.03}_{-0.02}$	0f	$5.89^{+2.06}_{-0.55}$	0.1f	$3.5^{+2.2}_{-2.3}$	72	29.0/21(1.38)
9.3	$0.76^{+0.19}_{-0.05}$	$0.0^{+2.2}$	$3.7^{+2.2}_{-1.2}$	$0.59^{+0.07}_{-0.31}$	0f	$5.35^{+\infty}_{-3.05}$	0.1f	$1.7^{+4.6}_{-1.7}$	30	17.8/19(0.94)
<i>ASCA</i> 1994 Apr										
$14.0^{+0.2}_{-0.3}$	–	$0.3^{+0.1}_{-0.2}$	–	$1.00^{+0.05}_{-0.04}$	0f	$6.57^{+0.91}_{-0.46}$	$2.34^{+1.17}_{-0.56}$	$54^{+66}_{-20}$	1400	1611/1610(1.00)
$13.7^{+0.3}_{-0.4}$	$0.97^{+0.04}_{-0.03}$	$0.2^{+0.2}_{-0.1}$	$3.6^{+0.4}_{-0.5}$	$0.65^{+0.07}_{-0.07}$	0f	6.30f	0f	$1.3^{+1.5}_{-1.3}$	27	1609/1610(1.00)


**Figure 7.** The X-ray spectra of 3C 382 from *ASCA*, *EXOSAT* and *Ginga* (from top to bottom).

above the break becomes then similar that for the *Ginga* data.

We then consider the *ASCA* spectrum of 3C 382. We find that adding a soft excess (using a model with a broken power law) results in a slight improvement of the fit over the model with a single power-law continuum, as shown in Table 8. However, the two models yield vastly different results regarding the Fe K line. The single-power law model requires the line to be very strong,  $W_{\text{Fe}} \gtrsim 1$  keV, and very broad,  $\sigma_{\text{Fe}} \sim 2$ –3 keV (as found before by Reynolds 1997). The line flux is then  $\sim 15$  times larger than that in the *Ginga* data. Also, the spectral index is much softer than that observed from the source in all previous *EXOSAT* and *Ginga* observations (Ghosh & Soundararajaperumal 1992; Kaastra et al. 1991). The extremely large  $\sigma_{\text{Fe}}$  would require the line origin from reflection in inner parts of an accretion disk (e.g., Fabian et al. 1995), for which, however, the expected  $W_{\text{Fe}}$  is at least several times less. Also, the weakness of the continuum reflection seen in the *Ginga* data appears to rule out a reflecting inner disk.

However, the Fe K line becomes very weak as well as unresolved in the broken power-law model, and the hard power-law index becomes then similar to that observed before by *EXOSAT* and *Ginga*. Also, the line flux in the *ASCA* observation becomes then compatible within statistical errors with that measured by *Ginga*. The line parameters are

not constrained due to the weakness of the line, and thus  $E_{\text{Fe}}$  and  $\sigma_{\text{Fe}}$  have been fixed at the best-fit values while determining the confidence regions of other parameters in this fit (Table 8). Since the *Ginga* data show reflection to be very weak, we do show here results of a fit with Compton reflection. The resulting line profile is shown in Figure 3.

We interpret the similar  $\chi^2$  in both above fits to the *ASCA* data as simply due to the very broad and strong Fe K line in the first fit giving the dominant *continuum* component above 7 keV, whereas that continuum is accounted for by the harder power law in the second fit. This discrepancy illustrates the importance of careful modeling of the continuum for determination of parameters of Fe K lines in *ASCA* data, which energy range extends only slightly above the energy range dominated by the Fe K line.

We have also analyzed the *ASCA* SIS data of 3C 382 obtained in the bright mode, which results in a substantially longer exposure for the SIS detectors but somewhat worse energy resolution (see Section 2). We have found that the results reported in Table 8 remain virtually unchanged. In particular the broken power law model yields only a narrow and weak Fe K line with the best-fit  $\sigma_{\text{Fe}} = 0$  keV and  $W_{\text{Fe}} = 28$  eV. However, another minimum with almost the same  $\chi^2$  is present, at which the line is broad with  $\sigma_{\text{Fe}} \simeq 1.4$  keV and  $W_{\text{Fe}} = 230$  eV. This would suggest that reflection from an inner disk may be present. However, when  $\Omega/2\pi$  is fixed at 1, corresponding to disk reflection, the line width becomes constrained to  $\sigma_{\text{Fe}} \lesssim 0.6$  keV with the best fit at  $\sigma_{\text{Fe}} \sim 0$  keV and  $W_{\text{Fe}} \simeq 30$  eV. Thus, the presence of a strong and broad Fe K line appears unlikely.

Figure 7 shows that the X-ray continuum of 3C 382 is strongly variable, with the 2-keV flux changing by an order of magnitude between the *Ginga* and *ASCA* observations. The spectral variability is similar to that seen 3C 390.3, namely the spectrum softens with increasing X-ray flux as well as the Fe K line flux is, within the statistical errors, compatible with constant. The line is thus unlikely to be due to reflection from an inner disk, and probably originates at large distances where the variable continuum is averaged due to large light-travel time across the region of line formation. However, the Fe K line-emitting region has to be out of the line of sight as the line strength is much too large (M86) to be due to the weak absorption in this object.

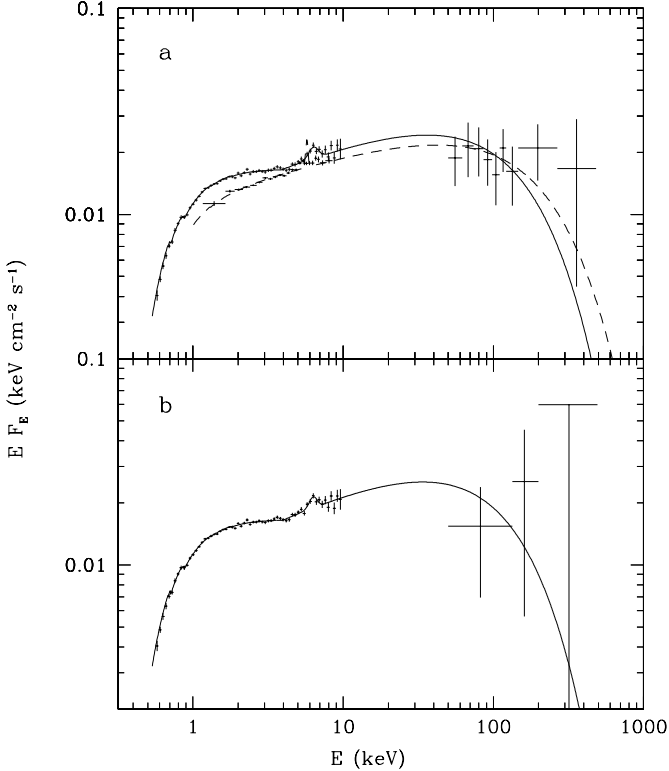


**Figure 8.** (a) The spectra of 3C 120 from *ASCA* (the upper X-ray spectrum), *EXOSAT* (the lower X-ray spectrum), and *OSSE* ( $> 50$  keV). The solid and dashed curves correspond to model with a broken power law and an exponential cutoff fitted to the *ASCA/OSSE* and *EXOSAT/OSSE* data, respectively. (b) The spectrum of 3C 120 from contemporaneous observations by *ASCA* (1994 February 17) and *OSSE* (1994 February 17–March 1). The same model form as in (a) was fitted to the data.

#### 4.5 3C 120

3C 120 is a BLRG exhibiting characteristics intermediate between those of FR I galaxies and BL Lacs (Urry & Padovani 1995). It is highly variable in all energy bands, and shows superluminal motion in the VLBI core (Muxlow & Wilkinson 1991; Walker, Benson & Unwin 1988; Walker, Walker & Benson 1988).

3C 120 has been observed by *EXOSAT* (Maraschi et al. 1991) and *ASCA*, but not by *Ginga*. Thus, we have no reliable information as yet on the presence of Compton reflection in this object. 3C 120 was observed by *HEAO-1*, and the A2 data imply a reflector solid angle of  $\Omega \simeq (1_{-1}^{+3}) \times 2\pi$  (rescaling the results of Weaver, Arnaud & Mushotzky 1995 obtained for angle-averaged reflection into an inclination of  $30^\circ$ ), i.e., the measurement errors are large for those data. Also, the A2 results for reflection in other AGNs (Weaver et al. 1995) correspond to solid angles systematically larger than those from *Ginga* (NP94). Taking into account those uncertainties, we compute below the spectral parameters for *ASCA* and *EXOSAT* data for both  $\Omega = 0$  and  $\Omega/2\pi = 1$ .

Table 9 gives fit results to the *ASCA* spectrum. Similarly to the case of 3C 382, we find the fitted line parameters depend very strongly on the way the continuum is modeled. If we model the *ASCA* continuum as a single power law, the

line is very strong,  $W_{\text{Fe}} \simeq 1$  keV, and broad,  $\sigma_{\text{Fe}} \simeq 2$  keV (as obtained before by Reynolds 1997). On the other hand, the line strength becomes moderate,  $W_{\text{Fe}} \simeq 100$  eV, and relatively narrow, when the power-law continuum is allowed to break. The spectrum corresponding to the latter model is plotted in Figure 8a. Allowing a break in the power law also improves the fit at the significance of 99.6 per cent. Thus, the very strong and broad line obtained for a single power-law fit seems to be an artefact of underestimating the continuum around the line in this model.

The presence of a soft excess in 3C 120 is confirmed by Grandi et al. (1997), who analyzed *ROSAT* PSPC observations from 1993. Those data, when fitted by a power law, show  $\alpha \sim 2-3$  in the 0.15–2.1 keV range. This argues in favour of the broken power-law model for the *ASCA* data and against the reality of the very strong and broad Fe K line obtained assuming no soft excess. Also, the averaged *EXOSAT* data yield almost the same parameters for the broken-power law model as the *ASCA* data, although those parameters are only weakly constrained.

The line parameters depend somewhat on the presence of Compton reflection. Table 9 also presents results of a fit with the assumed  $\Omega/2\pi = 1$  to the 4–10 keV data. The line becomes then even weaker and narrower than for the broken-power law model without reflection. The confidence contours for  $E_{\text{Fe}}$  and  $\sigma_{\text{Fe}}$  and the line profile are shown in Figures 2 and 3, respectively. Note that this fit yields a small  $W_{\text{Fe}} \simeq 60$  eV, which is not compatible with theoretical predictions (GF91; Życki and Czerny 1994) for the line strength from this process of  $W_{\text{Fe}} \sim 150-200$  eV (unless the reflector is so strongly ionized that resonant absorption suppresses the line), which argues against  $\Omega/2\pi \gtrsim 1$  in 3C 120.

The *ASCA* spectrum of 3C 120 has also been fitted in the 3–10 keV range (without including reflection) by Nandra et al. (1997). They obtained a Gaussian line with  $\sigma_{\text{Fe}} = 0.74_{-0.27}^{+0.34}$  keV and  $W_{\text{Fe}} = 330_{-130}^{+200}$  eV, and the power law index of  $\alpha = 0.89_{-0.06}^{+0.08}$  (their confidence regions are for  $\Delta\chi^2 = 4.7$ ). To enable a precise comparison of the results, we have also performed a fit with a power-law model in the 3–10 keV range, and obtained results virtually identical to those for the broken power-law fit presented in Table 9, e.g.,  $\sigma_{\text{Fe}} = 0.28_{-0.16}^{+0.96}$  keV and  $W_{\text{Fe}} \simeq 100$  eV. Thus, we find the Fe K line to be significantly narrower and weaker than that found by Nandra et al. (1997) for the same model and the same energy range used. This difference is apparently caused by an older version of the *ASCA* response and effective area used by those authors (of 1995, whereas we use the release of 1997). To study the issue further, we have also used the *ASCA* data on 3C 120 obtained with the data processing package of 1996 March–April. We have found very little difference with respect to our current results, e.g.,  $\sigma_{\text{Fe}} = 0.26_{-0.17}^{+0.76}$  keV and  $W_{\text{Fe}} \simeq 90$  eV for the power-law model in the 3–10 keV range. This demonstrates the importance of updating the results on the Fe K line parameters obtained with the pre-1996 data-processing software.

This conclusion is further reinforced by a comparison of our results with those of Grandi et al. (1997). They have fitted the 0.6–10 keV *ASCA* spectrum with a broken power-law continuum model. They found the break energy of 4 keV, similarly to our results (Table 9). However, they obtained the parameters very similar to those of Nandra et al. (1997),  $\sigma_{\text{Fe}} = 0.71_{-0.25}^{+0.24}$  keV (in the source frame),  $W_{\text{Fe}} = 280_{-80}^{+160}$

**Table 9.** Results of fits to the *ASCA* and *EXOSAT* spectra of 3C 120. The fit with Compton reflection to the *ASCA* data is limited to the 4–10 keV range.

<i>A</i>	$\alpha_s$	$N_H$	$E_b$	$\alpha$	$\Omega/2\pi$	$E_{Fe}$	$\sigma_{Fe}$	$I_{Fe}$	$W_{Fe}$	$\chi^2/\text{dof}(\chi^2_\nu)$
<i>ASCA</i> 1994 Feb										
$17.0^{+0.2}_{-0.2}$	–	$0.5^{+0.1}_{-0.1}$	–	$1.02^{+0.02}_{-0.03}$	0f	$6.72^{+0.27}_{-0.23}$	$1.73^{+0.49}_{-0.41}$	$40^{+11}_{-10}$	1000	1393/1441(0.94)
$16.7^{+0.3}_{-0.3}$	$1.00^{+0.02}_{-0.01}$	$0.4^{+0.1}_{-0.1}$	$4.0^{+0.3}_{-0.3}$	$0.72^{+0.07}_{-0.06}$	0f	$6.44^{+0.18}_{-0.22}$	$0.32^{+0.76}_{-0.20}$	$5.3^{+3.0}_{-2.4}$	110	1383/1439(1.00)
$12.7^{+1.3}_{-1.0}$	–	0.4f	–	$0.82^{+0.06}_{-0.06}$	1f	$6.41^{+0.33}_{-0.21}$	$0.20^{+\infty}_{-0.20}$	$3.3^{+6.7}_{-1.7}$	63	580/617(0.90)
<i>EXOSAT</i> 1983–86										
12.0	–	$0.0^{+0.4}_{-0.08}$	–	$0.79^{+0.02}_{-0.02}$	0f	$5.90^{+0.38}_{-0.37}$	0.1f	$4.6^{+1.9}_{-2.0}$	91	23/22(1.05)
12.9	–	$0.4^{+1.0}_{-0.4}$	–	$0.88^{+0.04}_{-0.03}$	1f	$5.51^{+0.77}_{-0.59}$	0.1f	$2.4^{+2.1}_{-2.0}$	41	20/22(0.89)

eV, and  $\alpha = 0.88^{+0.10}_{-0.08}$ , i.e., a line much broader and stronger and the hard continuum softer than those found for the same model in Table 9. These differences can again be entirely explained by an earlier version of the processing software (of 1994) they used.

The *ASCA* observation was contemporaneous with an observation by OSSE data (VP 317, see Table 4). This allows us to study the presence of a high-energy cutoff in the spectrum. We used a continuum model consisting of a broken power law multiplied it by an exponential factor. The resulting X $\gamma$  spectrum is shown in Figure 8b. We see that a high-energy spectral break or cutoff is indeed present, with the an e-folding energy of  $E_c = 110^{+130}_{-50}$  keV. The fit with no cutoff yields  $\Delta\chi^2 = +12$ , which corresponds to the statistical significance of the presence of a cutoff (or a break) of 99.95 per cent. We have also used the sum of the OSSE data for VP 317 and 320 (see Table 4), and found similar results. The significance of the presence of a cutoff increases if Compton reflection is assumed to be present (although the best fit to the combined data is obtained at  $\Omega = 0$ ). Thus, the cutoff cannot be explained as an artefact of the spectral curvature introduced by the spectral component from Compton reflection. We note that our result differs from that of Grandi et al. (1997), who found no cutoff in the combined data. This difference is due to, first, the *ASCA* data best-fitted by them by a softer power law than ours (due to an older version of the processing software, see above), and, second, their 50–150 keV flux from OSSE higher by  $\sim 30$  per cent than that found by us (which difference we have not been able to explain).

We can further constrain the presence of a cutoff by using the average OSSE spectrum from 9 observations in 1992–97 (see Table 4), shown in Figure 8a. If we fit those data together with the *ASCA* data, we obtain  $E_c = 130^{+150}_{-40}$  keV. We also compare the average OSSE spectrum with the average *EXOSAT* spectrum from 14 observations in 1983–86, also shown in Figure 8a. The joint fit with an e-folded power-law model yields  $E_c = 200^{+100}_{-60}$  keV, confirming the presence of a spectral break between X-rays and soft  $\gamma$ -rays.

## 5 OVERALL PROPERTIES OF BROAD-LINE RADIO GALAXIES

### 5.1 Summary of individual properties

Table 10 presents main parameters of selected models fitted to the X-ray spectra in Section 4, and the significance of the presence of the Fe K line obtained using the *F*-test. It

also gives the e-folding energies obtained using the available OSSE data, and the corresponding X $\gamma$  intrinsic luminosities. We see that the continuum Compton reflection is either absent or weak but the Fe K line flux is often much stronger than that expected from the weak reflection. Furthermore, this is the case in both objects with weak absorption in the line of sight and in 3C 445, which has strong ( $N_H \gtrsim 10^{23}$  cm $^{-2}$ ) absorption.

In 3C 445, the Fe K line can be explained entirely by absorption, and Compton reflection is constrained to be weak,  $\Omega/2\pi \lesssim 0.2$ . In 3C 111,  $\Omega/2\pi \lesssim 0.4$ , and the flux in the Fe K line can be in principle explained by the sum of the contributions from the observed absorption and Compton reflection. The only object with Compton reflection detected unambiguously is 3C 390.3, in which  $\Omega \sim 0.3$  was detected with a 99.99 per cent significance in one *Ginga* observation. However, the Fe K line strengths in two *ASCA* observations of this object were too large to be explained by that reflection (as well as absorption was negligible). In 3C 382,  $\Omega/2\pi \lesssim 0.3$  was obtained from the *Ginga* observation, but the line flux in that observation was much too large to be explained by either reflection or (negligible) absorption. In 3C 120, Compton reflection has not been measured. However,  $\Omega/2\pi \sim 1$  appears unlikely based on the weakness of the Fe K line implied by a model with strong reflection.

The observed variability also indicates the origin of the Fe K line different than from Compton reflection from an accretion disk. Namely, the line flux in repeated observations of 3C 390.3 and 3C 382 over several years by *Ginga* and *ASCA* is compatible with being constant whereas the flux around 10 keV changes within a factor of several. This disagrees with the origin of the line from the hard X-ray continuum incident on an accretion disk.

Furthermore, all but one *ASCA* observations show the lines are consistent with being unresolved with respect to the continua fitted above  $\sim 3$  keV. Thus, these data provide no compelling argument for the origin of the lines in inner accretion disks, consistent with the weakness of reflection and the lack of line variability. A possible exception is 3C 120, in which the broken-power law model without reflection yields the line being moderately broad, see Table 10. We note that if the 0.5–10 keV continuum in 3C 382 and 3C 120 is forced to be a single power law, the fitted lines become resolved and much stronger, with  $\sigma_{Fe} \sim 2$  keV and  $W_{Fe} \sim 1$  keV. However, this appears to be an artefact of neglecting the soft X-ray excesses present in BLRGs (observed by, e.g., *EXOSAT* and *ROSAT*).

Table 10 also shows results of fitting the X-ray data of 3 objects together with the OSSE data (not simultaneous)

**Table 10.** Summary of main parameters of BLRGs. The statistical significance of the presence of an Fe K line is given by  $P$ , where  $1 - P$  given below is the probability that there is no line in the data. The e-folding energy,  $E_c$ , is obtained using the average OSSE data when the data exist and assumed to be 400 keV otherwise, and  $L$  is the absorption-corrected 1–1000 keV isotropic luminosity corresponding to that model in units of  $10^{44}$  erg  $s^{-1}$  (assuming  $H_0 = 75$  km  $s^{-1}$  Mpc $^{-1}$ ).

Object	Instrument	$\alpha$	$\Omega/2\pi$	$W_{\text{Fe}}$	$\sigma_{\text{Fe}}$	$1 - P$	$E_c$ [keV]	$L$
3C 445	<i>Ginga</i>	$0.45^{+0.14}_{-0.10}$	$0^{+0.22}$	150	0.1f	–	400f	13.5
	<i>ASCA</i>	$0.39^{+0.28}_{-0.29}$	0f	140	$0^{+0.18}$	$1.4 \times 10^{-3}$	400f	29.4
3C 111	<i>Ginga</i>	$0.82^{+0.08}_{-0.06}$	$0.12^{+0.31}_{-0.12}$	78	0.1f	0.037	$1600^{+∞}_{-1300}$	10.0
	<i>ASCA</i>	$0.73^{+0.03}_{-0.02}$	0.12f	25	$0^{+∞}$	0.73	$300^{+130}_{-130}$	9.2
3C 390.3	<i>Ginga</i>	$0.90^{+0.03}_{-0.03}$	$0.35^{+0.15}_{-0.24}$	67	0.1f	$4.7 \times 10^{-4}$	$400^{+580}_{-170}$	11.6
		$0.70^{+0.09}_{-0.08}$	$0.26^{+0.37}_{-0.26}$	86	0.1f	0.013	$300^{+420}_{-120}$	9.0
	<i>ASCA</i>	$0.54^{+0.05}_{-0.07}$	0f	150	$0.10^{+0.12}_{-0.10}$	$5.6 \times 10^{-8}$	$260^{+320}_{-110}$	7.8
		$0.70^{+0.04}_{-0.03}$	0.35f	120	$0^{+0.33}$	0.016	$620^{+3600}_{-350}$	8.7
		$0.77^{+0.03}_{-0.03}$	0.35f	84	$0.20^{+∞}_{-0.20}$	0.28	$300^{+300}_{-110}$	9.8
3C 382	<i>Ginga</i>	$0.50^{+0.06}_{-0.04}$	$0.05^{+0.28}_{-0.05}$	220	0.1f	$1.0 \times 10^{-5}$	400f	8.4
	<i>ASCA</i>	$0.65^{+0.07}_{-0.07}$	0f	25	$0^{+∞}$	0.57	400f	17.2
3C 120	<i>ASCA</i>	$0.72^{+0.07}_{-0.06}$	0f	110	$0.32^{+0.76}_{-0.20}$	$3.0 \times 10^{-5}$	$130^{+150}_{-40}$	3.8

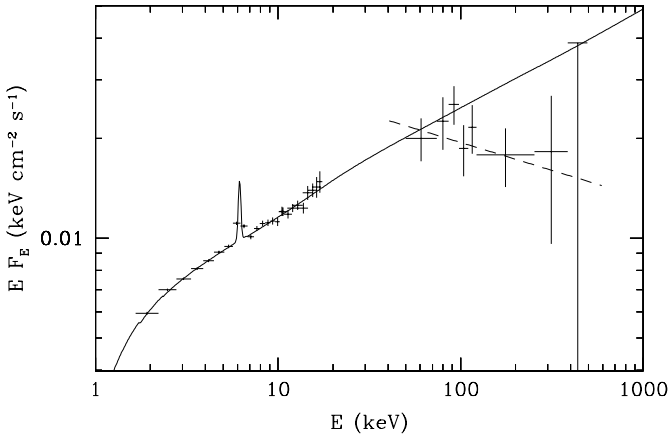


**Figure 9.** The average *Ginga* spectrum of 3C 111, 3C 382, and 3C 390.3, and the average OSSE spectrum of 3C 111, 3C 120, and 3C 390.3. The *Ginga* spectrum is fitted by the model with a power-law incident continuum plus Compton reflection and the Fe K line (solid curve). The dashed curve gives the power-law fit to the OSSE spectrum.

with an e-folded power law continuum. We note that in *all* cases, the OSSE data lie on or below the extrapolated X-ray continuum (initially fitted without the OSSE data), in spite of strong variability of both the X-ray flux and spectral index. This argues strongly for the presence of soft  $\gamma$ -ray spectral breaks in those spectra.

## 5.2 The average X-ray properties

The average hard X-ray spectral index of the studied objects is  $\sim 0.7$  for observations by all the three considered instruments, *Ginga*, *ASCA*, and *EXOSAT*. When Compton reflection is included, the average  $\alpha$  from the *Ginga* observations is 0.67 with a dispersion of 0.18. Similar values are obtained for the *EXOSAT* and *ASCA* observations. Only the *Ginga* data constrain the relative strength of Compton reflection. The unweighted average for the 5 observations of the 4 BLRGs is  $\Omega/2\pi = 0.16$ .

Very similar results to those above are also obtained for

the average *Ginga* spectrum of BLRGs, see Figure 9 and Table 11 (excluding 3C 445 due to the contamination of its spectrum by a cluster as well as due to its strong intrinsic absorption). The average values of  $z$  and  $N_{\text{H,G}}$  for the sample have been used. If only the top-layer *Ginga* data are used,  $\Omega = 0.09^{+0.25}_{-0.09}$  is found, i.e., very similar to that given in Table 11.

We stress that the average continuum properties of our sample are thus distinctly different from those of the sample of Seyfert 1s of NP94, which is strongly dominated by radio-quiet objects (although it also includes 3C 111, 3C 382, and 3C 390.3). For those objects, the average  $\alpha = 0.95$  with a dispersion of 0.15 and the average solid angle of the Compton reflector (in fits with a Fe K line independent of the continuum reflection) is  $\Omega/2\pi = 0.52$  with a dispersion of 0.18. So the two samples are distinctly different statistically.

In spite of the weak reflection in BLRGs, the *Ginga* and *ASCA* data show in many cases strong Fe K lines in the spectra, with the average equivalent width of 100 eV. This equivalent width clearly cannot be explained by the weak Compton reflection observed (e.g., GF91).

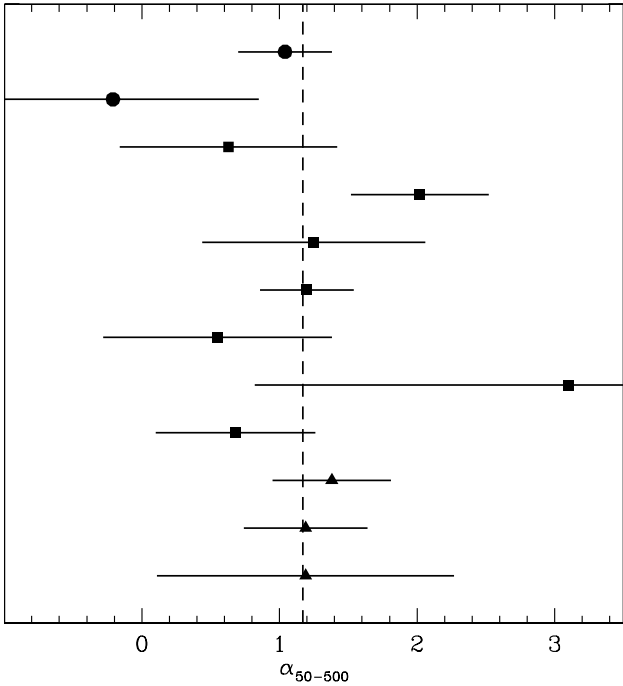
## 5.3 The soft $\gamma$ -ray properties

OSSE has observed 3 BLRGs until 1997, see Table 4. Table 4 also gives the values of the spectral index for fits with a power law, which are plotted in Figure 10. Although the individual determinations of  $\alpha$  bear large statistical errors, both the average  $\alpha = 1.17 \pm 0.16$ , and the  $\alpha$  fitted to the average OSSE spectrum, see Table 11 and Figure 9, are significantly larger than the X-ray spectral indices. Since Compton reflection is weak in BLRGs, the difference between the spectral indices clearly shows the existence of a break around  $\sim 100$  keV in the intrinsic soft  $\gamma$ -ray spectrum, see Figure 9.

Interestingly, the average OSSE spectrum of BLRGs is itself fully consistent with a power law and does not show any evidence for curvature. When the power law model is replaced by an e-folded power law, there is no improvement of the fit ( $\Delta\chi^2 = -1$  for addition of one parameter). Thus, there is no evidence for a high-energy cutoff in the power law above  $\sim 100$  keV (apart from the spectral break at that

**Table 11.** Fits to the average *Ginga*, OSSE and *EXOSAT* spectra of BLRGs.

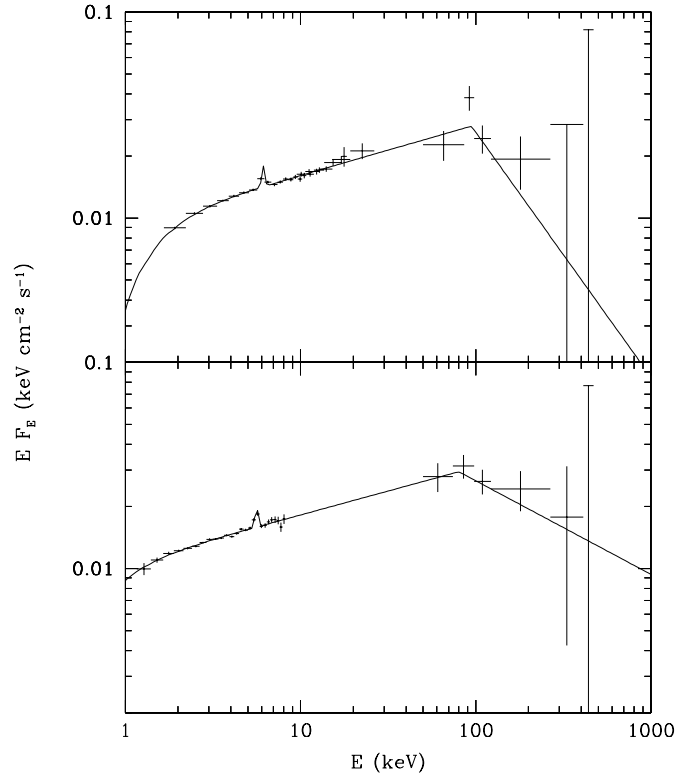
$A$	$\alpha$	$N_{\text{H}}$	$E_{\text{b}}$	$\Omega/2\pi$	$\alpha_{\text{h}}$	$E_{\text{Fe}}$	$I_{\text{Fe}}$	$W_{\text{Fe}}$	$\chi^2/\text{dof}(\chi^2_{\nu})$
Average <i>Ginga</i>									
5.5	$0.67^{+0.05}_{-0.04}$	$1.5^{+1.0}_{-1.1}$	–	$0.08^{+0.17}_{-0.08}$	–	$6.49^{+0.13}_{-0.14}$	$3.4^{+0.7}_{-0.7}$	130	35/34(1.02)
Average OSSE									
46.7	–	–	–	0f	$1.15^{+0.25}_{-0.28}$	–	–	–	35/38(0.97)
<i>Ginga</i> /OSSE									
9.2	$0.76^{+0.02}_{-0.02}$	$2.5^{+0.7}_{-0.7}$	$95^{+20}_{-25}$	0f	$2.14^{+3.10}_{-0.90}$	$6.46^{+0.18}_{-0.17}$	$3.1^{+0.9}_{-0.8}$	80	50/78(0.65)
<i>EXOSAT</i> /OSSE									
10.6	$0.77^{+0.02}_{-0.02}$	0f	$80^{+35}_{-73}$	0f	$1.52^{+1.20}_{-0.55}$	$5.9^{+0.4}_{-0.5}$	$3.9^{+1.9}_{-1.9}$	76	49/54(0.90)
Average <i>Ginga</i> /average OSSE									
5.4	$0.67^{+0.02}_{-0.02}$	$1.2^{+1.0}_{-0.7}$	$93^{+20}_{-28}$	0f	$1.66^{+1.02}_{-0.55}$	$6.47^{+0.14}_{-0.13}$	$3.4^{+0.8}_{-0.7}$	130	66/70(0.94)


**Figure 10.** The distribution of the 50–500 keV energy spectral index in OSSE observations of BLRGs. The vertical dashed line corresponds to the weighted average of  $\alpha$ . The filled circles, squares and triangles with error bars correspond to the fits in Table 4 for 3C 111, 3C 120, and 3C 390.3, respectively.

energy implied by the extrapolated X-ray spectra). This contrasts the case of radio-quiet Seyferts 1s and 2s, which average OSSE spectra show spectral curvature at very high significance:  $\chi^2_{\nu} = 1.4$  for a power law fit and 0.9 for an e-folded power law fit (Johnson et al. 1997).

A break at  $\sim 100$  keV is also indicated by the simultaneous *ASCA*/OSSE observation of 3C 120 (see Section 4.5). To further constrain the presence of a break, we have also obtained the average X $\gamma$  spectra of BLRGs observed by both *Ginga* and OSSE (3C 111 and 3C 390.3; Z95), and *EXOSAT* and OSSE (3C 120 and 3C 390.3). In fits, we use the average values of  $z$  and  $N_{\text{H,G}}$  from Table 1 for each pair. Since the number of OSSE observations is limited for those samples, we allow for free normalization of the OSSE data with respect to the other data sets.

We have fitted the spectra with e-folded power laws


**Figure 11.** The average spectrum of 3C 111 and 3C 390.3 from *Ginga*/OSSE (top) and of 3C 120 and 3C 390.3 from *EXOSAT*/OSSE (bottom). The solid curves correspond to the model with a broken power law and an Fe K line.

and Compton reflection, and with broken power laws, and found that the latter model provides a better fit ( $\Delta\chi^2 = -6$  and  $-2$  for *Ginga*/OSSE and *EXOSAT*/OSSE, respectively). Results of the fits with that model are given in Table 11 and Figure 11 (the *EXOSAT*/OSSE data are best-fitted with  $N_{\text{H}} = 0$ ). The fits confirm the presence of breaks in those spectra around  $\sim 100$  keV although the form of the break is relatively poorly constrained. A single power-law model is ruled out at a high significance,  $\Delta\chi^2 = +10$  and  $+6$  for the *Ginga*/OSSE and *EXOSAT*/OSSE data, respectively.

Finally, we also fit together the average *Ginga* and OSSE spectra of all available objects, shown in Figure 9, see the last row of Table 11. Again an e-folded power law model provides a worse fit than a broken power law, and the break energy is at  $\sim 100$  keV.

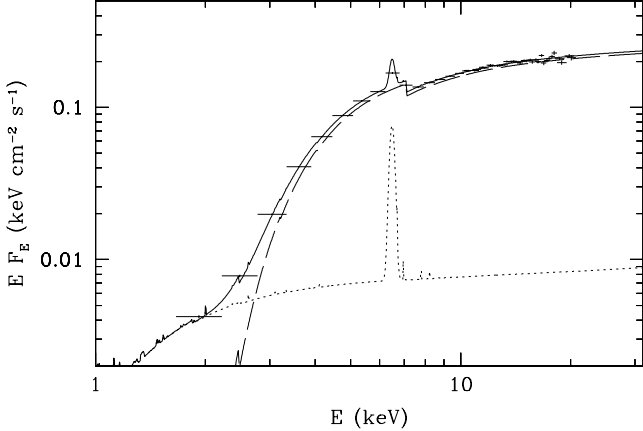


**Figure 12.** The *Ginga* spectrum of Cen A (crosses). The dashed curve represents the absorbed hard X-ray power law, and the dotted curve gives the sum of components dominant at soft X-rays (see text) and the Fe K line. The solid curve gives the sum. No Compton reflection is found in the best fit of this model.

## 6 COMPARISON WITH Cen A

Cen A (NGC 5128) is the nearest active galaxy at  $z = 0.0008$  and with  $N_{\text{H,G}} = 7 \times 10^{20} \text{ cm}^{-2}$  (Stark et al. 1992). No broad line emission can be observed from this giant elliptical radio galaxy due to heavy absorption in a warped dusted lane viewed close to edge-on, and thus it is not a BLRG. On the other hand, the unified AGN model (e.g., Antonucci 1993) postulates that the difference between AGNs with and without broad lines is solely due to the viewing angle of the nucleus. Since Cen A is one of the the brightest extragalactic X-ray sources, we can determine with high accuracy its  $X\gamma$  properties despite the relatively large absorbing column density, in particular, the presence of Compton reflection and a high-energy break. We can then compare these properties with those obtained in this work for BLRGs, with the goal to test the unified AGN model.

We use here the *Ginga* spectrum of Cen A of 1989 March 8 (Miyazaki et al. 1996; Warwick et al. 1998). We note that Cen A exhibits a strong and complex soft X-ray spectrum. To account for that, we include fixed soft X-ray components due to the jet and diffuse emission (observed by *ROSAT*) as a soft power law and 2 hot-plasma components following Turner et al. (1997). The primary nuclear continuum is modeled by a power law including reflection absorbed by a column,  $N_{\text{H},1}$ . The viewing angle of the reflection component is taken as  $70^\circ$  (Graham 1979; Dufour et al. 1979). The nucleus continuum itself shows a soft X-ray excess, which we model here as a power law with the same  $\alpha$  but absorbed by a lower column,  $N_{\text{H},2}$ , following Warwick et al. (1998) and Turner et al. (1997). This provides a good fit to the *Ginga* spectrum, and fit results are presented in Table 12. We see that Compton reflection is at most weak, similar to results of Miyazaki et al. (1996) and Warwick et al. (1998). (If only the top-layer data are used,  $\Omega/2\pi = 0^{+0.15}$ , identical to the result in Table 12.) The Fe K line in the spectrum can be explained as due to fluorescence in the absorbing column,  $N_{\text{H}}$  (M86). Note that when the Fe  $K\beta$ /Ni  $K\alpha$  lines are included in the model (as for the *ASCA* data, Section 3),  $E_{\text{Fe}} \simeq 6.4 \pm 0.1 \text{ keV}$  and  $\sigma_{\text{Fe}} \simeq 0^{+0.4}$

keV. The line is thus compatible with being narrow, as confirmed using *ASCA* data by Turner et al. (1997). We also note that our results on the hard continuum are rather independent of the assumed form of the soft X-ray excess, which is only weakly constrained by the *Ginga* data. For example, we have obtained almost identical results as above by modeling the entire soft component as bremsstrahlung at  $kT = 1.65 \text{ keV}$ , which was used in fitting *EXOSAT* data on Cen A by Morini, Anselmo & Molteni (1989).

OSSE observed repeatedly Cen A during 1991–94 (Kinzer et al. 1995). The soft  $\gamma$ -ray flux varied within a factor of two. All the spectra showed distinct spectral breaks. When the spectra were fitted with a broken power law, the break energy was  $\sim 140\text{--}170 \text{ keV}$ . The power law below the break was  $\alpha \sim 0.7$  (only slightly harder than that seen by *Ginga* in 1991). A similar break energy of  $180 \text{ keV}$  was found in a balloon observation (Miyazaki et al. 1996). The hard power law seen by OSSE above the break was found to continue without any further break to  $\sim 10 \text{ MeV}$  by the COMPTEL detector aboard *CGRO* (Steinle et al. (1997), as illustrated in Fig. 6 of Johnson et al. (1997). However, a spectral softening above  $\sim 10 \text{ MeV}$  is required by the  $\geq 100 \text{ MeV}$  flux measured from Cen A by EGRET (see Steinle et al. 1997).

Thus, we find that the X-ray spectral index, the tight limit on Compton reflection, and the spectral break around  $\sim 150 \text{ keV}$  in Cen A are very similar to those found in our sample of BLRGs. (Unfortunately, no useful constraints on the spectra above  $1 \text{ MeV}$  can be obtained for BLRGs). This similarity is strongly suggestive of the common nature of the radiative processes in both narrow-line and broad-line radio galaxies, as expected in the AGN unified model.

## 7 DISCUSSION

### 7.1 The origin of the Fe $K\alpha$ line

Our results clearly show that the bulk of the Fe K line flux in our sample of BLRGs is unlikely to be due to Compton reflection, which is weak (or absent) in the studied objects. In 3C 445, the line can be satisfactorily explained by strong absorption in the line of sight, with  $N_{\text{H}} \gtrsim 10^{23} \text{ cm}^{-2}$ . This is also the case in our comparison narrow-line object, Cen A. On the other hand, absorption in the line-of-sight in 3C 111, 3C 120, 3C 382, and 3C 390.3 is too weak to be able to explain the observed line fluxes.

However, the observed line fluxes can be satisfactorily explained in those objects if there is matter with  $N_{\text{H}} \gtrsim 10^{23} \text{ cm}^{-2}$  covering a large solid angle,  $\Omega_o$ , *outside* our line of sight. Such matter can be identified with molecular torii, common in AGNs. Irradiation of this matter by a power law spectrum with the 1-keV normalization,  $A$ , and the energy spectral index,  $\alpha$ , gives rise to a flux in the Fe K line of approximately

$$I_{\text{Fe}} \approx \frac{1.7A_{\text{Fe}}}{\alpha + 3} \frac{\Omega_o}{4\pi} Y A \min\left(\tau_{\text{T}}, \frac{0.5}{A_{\text{Fe}}}\right) \frac{(1 \text{ keV})^{1+\alpha}}{E_{\text{K}}^\alpha}, \quad (1)$$

where  $1.7A_{\text{Fe}}$  is the ratio of the Fe K-edge cross section (at  $E_{\text{K}}$ ) times the relative Fe abundance to the Thomson cross section,  $Y \sim 1/2$  is the fluorescence yield, and  $\tau_{\text{T}}$  is the Thomson optical depth of the medium (see Krolik & Kallman 1987). At  $\tau_{\text{T}} \gtrsim 0.5/A_{\text{Fe}}$ , the K-edge optical



**Table 12.** Results of the fit to the *Ginga* spectrum of Cen A. The model also includes 3 fixed components, see text.  $W_{\text{Fe}}$  is given with respect to the total absorbed continuum.

$A_i$	$N_{\text{H},i}$	$\alpha$	$\Omega/2\pi$	$E_{\text{Fe}}$	$\sigma_{\text{Fe}}$	$I_{\text{Fe}}$	$W_{\text{Fe}}$	$\chi^2/\text{dof}(\chi^2_{\nu})$
$120^{+10}_{-10}, 4.5^{+3.5}_{-1.6}$	$170^{+10}_{-10}, 10.0^{+1.2}_{-1.0}$	$0.79^{+0.06}_{-0.05}$	$0^{+0.15}$	$6.49^{+0.11}_{-0.11}$	0.1f	$42^{+8}_{-9}$	$130^{+25}_{-25}$	40/39(1.03)

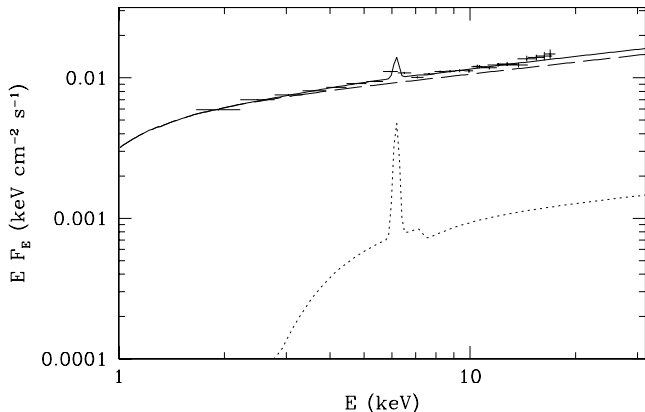


**Figure 13.** A contribution to the spectrum of a BLRG (as illustrated by the average *Ginga* spectrum) from Thomson scattering in a medium with  $N_{\text{H}} = 2 \times 10^{23} \text{ cm}^{-2}$  covering a  $3\pi$  solid angle as seen from the nucleus (dotted curve). The medium is outside of the line of sight and thus it does not absorb the direct continuum with assumed no reflection (dashed curve). The solid curve gives the sum.

depth exceeds unity and the line flux approximately saturates. For the average *Ginga* spectrum of BLRGs (Table 11),  $(\Omega_o/4\pi)A_{\text{Fe}}\tau_{\text{T}} \simeq 0.1$  is required to account for the observed Fe K line. This is compatible with the  $N_{\text{H}}$  observed in 3C 445 and Cen A.

Such a medium will also give rise to a scattered continuum component, approximately given by  $(\Omega_o/4\pi)\tau_{\text{T}} \exp[-\tau_{\text{bf}}(E)]$  times the observed direct continuum, where  $\tau_{\text{bf}}(E)$  is the bound-free optical depth of the surrounding medium. The presence of such a continuum component is allowed by the X-ray data (but only weakly constrained). Figure 13 shows an example of the scattered spectrum (the dotted curve) for  $N_{\text{H}} = 2 \times 10^{23} \text{ cm}^{-2}$  and  $\Omega_o \simeq 3\pi$ . We see that although this component contributes only weakly to the total continuum it accounts entirely for the Fe K line. We note that the scattered component does not have the shape characteristic to Compton reflection (with a fast increase of its relative contribution around 10 keV). Thus, the weak Compton reflection still present in the X-ray spectra of BLRGs cannot be explained by scattering in the surrounding optically-thin matter (see Section 7.2 below).

We note that the surrounding medium will be, most likely, partly photo-ionized. For an ionizing luminosity typical for a BLRG in our sample,  $L_{\text{ion}} \sim 5 \times 10^{44} \text{ erg s}^{-1}$ , and a distance between the nucleus and the medium with  $N_{\text{H}} \sim 2 \times 10^{23} \text{ cm}^{-2}$  of 5 pc, the ionization parameter (see Section 3) will be  $\xi \sim 100$ . Therefore, we assumed  $\xi = 100$  in the illustrative example in Figure 13. At a typical medium temperature of  $10^4 \text{ K}$ , the dominant Fe ion is found to be Fe xv, implying that resonant absorption of the line is negligible. We note that a range of ionization states in the line-

producing medium will give rise to some broadening of the line.

A possible complication in the scenario with production of Fe K photons outside of the line of sight can be due to beaming of the primary radiation (e.g., Awaki et al. 1991). Beaming is expected in jet emission, and radio jets are present in most of the sources in our sample. Such beaming will relax the constraint on  $(\Omega_o/4\pi)\tau_{\text{T}}$  discussed above. For example, we could explain the line in 3C 111 seen by *Ginga* as due to fluorescence in a medium with the *observed*  $N_{\text{H}}$  ( $\sim 2 \times 10^{22} \text{ cm}^{-2}$ ) if the irradiating flux is enhanced by a factor of  $\sim 100$  in a cone with the opening angle of  $15^\circ$ .

Summarizing, we find that the simplest explanation of the Fe K line observed in BLRGs is a distant torus with  $N_{\text{H}} \gtrsim 10^{23} \text{ cm}^{-2}$  covering a large solid angle as seen from the nucleus. More complex scenarios are, however, also compatible with the data.

## 7.2 The origin of the Compton reflection

A possible explanation of the apparent small solid angle of a Thomson-thick reflector,  $\Omega \ll 2\pi$ , is the primary emission originating in the vicinity of an accretion disk but collimated away from the disk. Collimation is expected in radio-loud AGNs, e.g., the X $\gamma$  emission of blazars certainly originates in a jet pointing away from the source plane. For mild collimation, e.g., one due to a subrelativistic outflow, the observed reduction of Compton reflection by a factor of a few (with respect to an isotropic source above a disk) can be easily achieved. In this scenario, the bulk of the Fe K line does not originate in the reflection region, but rather in a remote torus (as argued in Section 7.1 above). Then we can explain both the approximate constancy with time of the line flux (from the remote torus) as well as constant relative weakness of the continuum reflection (from the disk close to the primary X-ray source). We note that *some* short time-scale variability of the line flux is predicted due to the disk-line contribution (with the expected  $W_{\text{Fe}} \sim 30\text{--}50 \text{ eV}$  at the observed  $\Omega$ , e.g., GF91). Also, that disk-line component can be broad due to relativistic effects (e.g., Fabian et al. 1995).

Alternatively, the cold, reflecting, disk can be truncated at a large radius (in units of the Schwarzschild radius), due to, e.g., a disk instability. If the continuum source is located inside the truncation radius, the solid angle covered by the cold disk would be small. This scenario has been proposed to explain the weakness of Compton reflection in NGC 4151 (Zdziarski, Johnson & Magdziarz 1996).

The observed weak Compton reflection can also be possibly explained in the absence of a disk by reflection from the torus discussed in Section 7.1 above, provided  $N_{\text{H}} \sim 10^{24} \text{ cm}^{-2}$  (Krolik, Madau & Życki 1994; Ghisellini, Haardt & Matt 1994). At this  $N_{\text{H}}$  there will be already a signature of spectral hardening above  $\sim 10 \text{ keV}$ , but the resulting reflection spectral component will be substantially weaker than

that from a medium with  $N_{\text{H}} \gg 10^{24} \text{ cm}^{-2}$ . This scenario requires some fine-tuning of  $N_{\text{H}}$  and  $\Omega_{\text{o}}$  but it is in principle possible. Note that in that case both the Fe K line and the reflection arise in the same region and a correlation on long time scales between  $I_{\text{Fe}}$  and  $\Omega$  would be present. The data presented here are insufficient to test for the presence of such correlation.

Finally, the weakness of Compton reflection could in principle be due to the dilution of the standard Seyfert-1 component with strong reflection by another component, e.g., from a comparatively low-luminosity blazar-like jet pointing close to our line of sight. This, in principle, would be supported by the detection of superluminal expansion in the radio images (see Section 4). However, the X-ray data do not support such a picture. First, the observed large fluxes of the  $\text{K}\alpha$  line cannot be directly explained in this scenario. Second, we have found that the data above  $\sim 2$  keV do not allow the presence of a substantial second continuum component. We have considered a continuum model consisting of a power law with a free spectral index plus a (radio-quiet) Seyfert-1-like continuum with fixed  $\alpha = 0.95$  and  $\Omega/2\pi = 0.52$ , i.e., the average values obtained by NP94. The line strength was not tied to either component. We have found that such a 2-component model provides a fit to the average *Ginga* spectrum *worse* than the single power-law plus reflection model used throughout this paper. The best fit to the 1-keV normalization of the Seyfert-1 continuum is null, and its upper limit is 2 per cent of the power-law normalization (at 90 per cent confidence). Even the upper limit would imply the reflection component much weaker than the observed  $\Omega/2\pi \sim 0.1\text{--}0.3$ . Thus, Compton reflection with this  $\Omega$  observed in BLRGs cannot be explained as due to dilution of the Seyfert-1-like X-ray spectrum by another spectral continuum. This conclusion is supported for 3C 390.3 by observations of a pattern of X-ray variability implying a single X-ray source (Leighly & O'Brien 1997).

### 7.3 The origin of the continuum and the high-energy break

As found in the Section 7.2 above, the intrinsic X-ray continua of BLRGs are unlikely to be composed of two components, e.g., one from the nucleus and one from a jet. Thus, the X-ray continuum in a BLRG appears to originate predominantly in a single emission source. This region may be either similar to that present in radio-quiet Seyfert 1s, or be related to an X $\gamma$  jet, as in blazars. In any case, the observed continuum emission has to be much more isotropic than in blazars at least in 3C 390.3, as shown by a Compton reflection component clearly detected in that BLRG. An important diagnostic for the nature of the continua can also be provided by the high-energy spectral breaks observed in the spectra.

We found that the presence of high-energy breaks in the spectra of BLRGs is established based on: (i) the break in the simultaneous *ASCA*/OSSE spectrum of 3C 120, (ii) the breaks seen in the average spectra of BLRGs observed repeatedly by both *Ginga* and OSSE and by both *EXOSAT* and OSSE, and (iii) the average spectra of all BLRGs observed by OSSE being much softer than both the individual X-ray spectra and the average *Ginga* and *EXOSAT* spectra. Furthermore, a similar break is clearly seen in Cen A (Kinzer

et al. 1995), a narrow-line object considered to differ from BLRGs mostly by orientation (e.g., Antonucci 1993). The spectra are seen to break above  $\sim 100$  keV, which is similar to the breaks seen in radio-quiet Seyfert 1s (Z95; Gondek et al. 1996; Zdziarski et al. 1996, 1997).

We note that although models with an e-folded power law provide worse spectral fits to the average X $\gamma$  spectra than the broken power law model (Section 5.3), there are no available simultaneous X $\gamma$  observations with statistics sufficient to distinguish between different shapes in soft  $\gamma$ -rays of individual spectra. A spherical thermal Comptonization model of Poutanen & Svensson (1996) including Compton reflection fitted to the average *Ginga*/average OSSE spectrum yields the electron temperature of  $kT_e \simeq 110$  keV and the optical depth of  $\tau \simeq 1.3$  at the best fit, although the fit is worse than that with the broken power-law model (without reflection, Table 11),  $\Delta\chi^2 = +3.4$ . A similar thermal Comptonization model fits well the X-ray to soft  $\gamma$ -ray spectra of radio-quiet Seyfert 1s (e.g., Zdziarski et al. 1997). That model can also explain the anti-correlation between the X-ray slope and the ratio between the X-ray to UV fluxes observed in 3C 120 (Walter & Courvoisier 1992). Thus, thermal Comptonization remains a possible explanation of the X $\gamma$  continua of BLRGs.

The relative hardness of the X-ray spectra in BLRGs with respect to radio-quiet Seyfert 1s can be related in the thermal Comptonization model to the relative weakness of Compton reflection in BLRGs. This can be explained as follows. In this model, the soft (UV/soft X-rays) seed photons are repeatedly upscattered by a hot plasma cloud to the hard X-ray/soft  $\gamma$ -ray range. In the case of radio-quiet Seyfert, the seed photons are from internal dissipation in an accretion disk as well as from reprocessing of the incident X $\gamma$  photons (e.g., Haardt & Maraschi 1993). On the other hand, the seed photon field produced from reprocessing is weak in BLRGs, as inferred from the weakness of the reflected component. The energy density of the seed photons in the plasma frame can be further Doppler-reduced if there is a sub-relativistic outflow of the plasma (see Section 7.2 above). From energy balance, the reduced supply of seed photons leads to reduced cooling and, consequently, to a hardening of the Comptonized X-ray spectrum (e.g., Poutanen & Svensson 1996). Physically, it can be realized, e.g., if the continuum source forms an inner hot accretion disk thermally Comptonizing cold radiation from the outer disk and cold clouds within the hot flow, and the reflection of the continuum is from the outer cold disk (see, e.g., Zdziarski 1998).

On the other hand, the X-ray and soft  $\gamma$ -ray spectra of BLRGs can be due to emission of nonthermal electrons. This possibility is hinted at by the apparent power-law shape (with no spectral curvature required) of the average OSSE spectrum of BLRGs (Section 5.3). Furthermore, the radio emission of BLRGs, and certainly that arising in the milli-arcsecond region, is nonthermal. The X-ray spectral slopes of blazars, which emission is certainly nonthermal, are similar to those found in BLRGs. Also, the blazar spectra universally show a high-energy spectral break, which energy, however, falls in the MeV range. The nature of the break is not understood yet (e.g., Sikora et al. 1997), but it is generally agreed upon that their jets show Lorentz factors  $\sim 10$ ; see Dondi & Ghisellini (1996). If the plasma in BLRGs propa-

gates with bulk velocities that are at most trans-relativistic, or, alternatively, they are viewed at a larger angles to the direction of motion – the spectral break in BLRGs could then appear at the appropriately lower energy,  $\sim 100$  keV.

Yet another process giving rise to a high-energy spectral break has been discussed by Skibo, Dermer & Kinzer (1994). They proposed that the high-energy break observed in Cen A above  $\sim 150$  keV (Kinzer et al. 1995) is due to the emission of a jet (beamed away from our line of sight) being Compton-scattered by a plasma cloud into our line of sight. The break appears due to the kinematics of scattering in the Klein-Nishina regime. This model, however, predicts the break energy at an energy  $\gtrsim 1$  MeV at the viewing angle of  $30^\circ$ , likely to be typical for broad-line objects such as BLRGs. To achieve a break around 100 keV, as observed for our sample, viewing angles of  $\gtrsim 70^\circ$  and relativistic motion of the scattering cloud are necessary (Fig. 1 in Skibo et al. 1994). Thus, this model appears to be ruled out for BLRGs. For Cen A itself, this model has difficulty in explaining the variability of the soft  $\gamma$ -ray flux on a time scale as short as 12 hours (Kinzer et al. 1995) and the high-energy power law extending to  $\sim 10$  MeV (Steinle et al. 1997).

The present difficulty of determining the nature of the high-energy break in BLRGs is mostly due to the relatively limited sensitivity of the present soft  $\gamma$ -ray detectors, e.g., OSSE. A progress in resolving this issue is likely after the launch of *INTEGRAL* (e.g., Winkler 1996), with its high sensitivity above 100 keV of the IBIS detector (Ubertini et al. 1996).

## 8 CONCLUSIONS

The data presented here allow the first systematic comparison of the X $\gamma$  properties of BLRGs with their radio-quiet counterparts, Seyfert 1s. Our main conclusions are as follows.

1. The intrinsic (i.e., both absorption and reflection-corrected) X-ray continua of BLRGs are harder on average than those of (radio-quiet) Seyfert 1s. The *Ginga* data presented here give the average  $\alpha = 0.67$  with a dispersion of 0.18, compared to the average  $\alpha = 0.95$  with a dispersion of 0.15 in all Seyfert 1s (NP94). Also, the relative strength of Compton-reflected continuum in BLRGs corresponds to the reflector solid angle of  $\ll 2\pi$  whereas the Seyfert-1 data yield significantly larger solid angles, on average of  $\sim (0.5-0.7) \times 2\pi$  (NP94). The *ASCA* and *EXOSAT* data on BLRGs presented here are fully compatible with the data from *Ginga*.

2. The flux in the Fe K line in BLRGs is in most cases stronger than that expected from the observed weak Compton reflection. The corresponding average line equivalent width is  $\sim 100$  eV. With a possible exception of 3C 120, the *ASCA* data are compatible with the Fe K line being unresolved. The line flux remains approximately constant in time in spite of the variable continuum in observations of individual objects spanning several years.

3. The simplest model of the origin of the Fe K flux is irradiation by the central X-ray source of a distant torus with  $N_{\text{H}} \gtrsim 10^{23}$  cm $^{-2}$ . The torus is away of the direct line of sight in the objects in our sample except for 3C 445, in

which X-ray absorption by such a column density is directly observed.

4. The data show a high-energy spectral break at  $\sim 100$  keV, which resembles that seen in radio-quiet Seyferts. The break can be explained by either thermal Comptonization or by nonthermal models, with the latter marginally favoured by the available data.

5. The main X $\gamma$  spectral properties of BLRGs: the hardness of the X-ray power law, weak reflection, and a high energy break above 100 keV, are also observed in the bright narrow-line radio galaxy, Cen A, which would be a BLRG viewed through the obscuring torus in the framework of the unified AGN model.

## ACKNOWLEDGEMENTS

This research has been supported in part by the KBN grants 2P03D00614, 2P03D01209, and 2P03C00511p0(1,4), and NASA grants and contracts. PRW acknowledges a scholarship from T. Chlebowski, Inc., for undergraduate studies in astronomy. We acknowledge the use of the NASA/GSFC HEASARC archive for the *ASCA* and *EXOSAT* data. We thank Julian Krolik and Marek Sikora for discussions, and Ian George, Marek Gierliński and Paweł Magdziarz for their valuable assistance with software used in this work.

## REFERENCES

- Anders E., Ebihara M., 1982, *Geochim. Cosmochim. Acta*, 46, 2363
- Antonucci R. R. J., 1993, *ARA&A*, 31, 473
- Arnaud K. A., 1996, in Jacoby G. H., Barnes J., eds, *ASP Conf. Ser. 101, Astronomical Data Analysis Software and Systems V.*, Astron. Soc. Pac., San Francisco, p. 17
- Awaki H., et al., 1991, *PASJ*, 43, 195
- Brinkmann W., Siebert J., Reich W., Fürst E., Reich P., Voges W., Trümper J., Wielebinski R., 1995, *A&AS*, 109, 147
- Colina L., Pérez-Fournon I., 1990, *ApJS*, 72, 59
- Done C., Mulchaey J. S., Mushotzky R. F., Arnaud K., 1992, *ApJ*, 395, 275
- Dondi L., Ghisellini G., 1996, *MNRAS*, 273, 583
- Dufour R. J., van den Berg S., Harvel C. A., Martins D. H., Schiffer F. H., III, Talbot R. J., Jr., Talent D. L., Wells D. C., 1979, *AJ*, 84, 284
- Eracleous M., Halpern J. P., Livio M., 1996, *ApJ*, 459, 89
- Fabian A. C., Nandra K., Reynolds C. S., Brandt W. N., Otani C., Tanaka Y., Inoue H., Iwasawa K., 1995, *MNRAS*, 277, L11
- George I. M., Fabian A. C., 1991, *MNRAS*, 249, 352 (GF91)
- Ghisellini G., Haardt F., Matt G., 1994, *MNRAS* 267, 743
- Ghosh K. K., Soundararajaperumal S., 1991, *AJ*, 102, 1298
- Ghosh K. K., Soundararajaperumal S., 1992, *ApJ*, 389, 179
- Gondek D., Zdziarski A. A., Johnson W. N., George I. M., McNaron-Brown K., Magdziarz P., Smith D., Gruber D. E., 1996, *MNRAS*, 282, 646
- Graham J. A., 1979, *ApJ*, 232, 60
- Grandi P., Sambruna R. M., Maraschi L., Matt G., Urry C. M., Mushotzky R. F., 1997, *ApJ*, 487, 636
- Haardt F., Maraschi L., 1993, *ApJ*, 413, 507
- Hayashida K., et al., 1989, *PASJ*, 41, 373
- Inda M., et al., 1994, *ApJ*, 420, 143
- Johnson W. N., Zdziarski A. A., Madejski G. M., Paciesas W. S., Steinle H., Lin Y.-C., 1997, in Dermer C. D., Strickman M. S., Kurfess J. D., eds, *The 4th Compton Symposium*, AIP, New York, p. 283

- Kaastra J. S., Kunieda H., Awaki H., 1991, *A&A*, 242, 27
- Kellermann K. I., Sramek R., Schmidt M., Shaffer D. B., Green R., 1989, *AJ*, 98, 1195
- Kinzer R. I., et al., 1995, *ApJ*, 449, 105
- Krolik J. H., Kallman T. R., 1984, *ApJ*, 286, 366
- Krolik J. H., Kallman T. R., 1987, *ApJ*, 320, L5
- Krolik J., Madau P., Życki P., *ApJ*, 420, L57
- Lawson A. J., Turner M. J. L., 1997, *MNRAS*, 288, 920
- Leighly K. M., O'Brien P. T., 1997, *ApJ*, 481, L15
- Leighly K. M., O'Brien P. T., Edelson R., George I. M., Malkan M. A., Matsuoka M., Mushotzky R. F., Peterson B. M., 1997, *ApJ*, 483, 767
- Lightman A. P., White T. R., 1988, *ApJ*, 335, 57
- Linfield R., Perley R., 1984, *ApJ*, 279, 60
- Magdziarz P., Zdziarski A. A., 1995, *MNRAS*, 273, 837
- Makishima K., 1986, in Mason K. O., Watson M. G., White N. E., eds, *The Physics of Accretion onto Compact Objects*, Springer, Berlin, p. 249 (M86)
- Malaguti G., Bassani L., Caroli E., 1994, *ApJS*, 94, 517
- Maraschi, L., Chiapetti L., Falomo R., Garilli B., Malkan M., Tagliaferri G., Tanzi E. G., Treves A., 1991, *ApJ*, 368, 138
- McDonald G.M., Kenderdine S., Neville A.C., 1968, *MNRAS*, 138, 259
- Miyazaki S., et al., 1996, *PASJ*, 48, 801
- Morini M., Anselmo F., Molteni D., 1989, *ApJ*, 347, 750
- Morrison R., McCammon D., 1983, *ApJ*, 270, 119
- Muxlow T. W. B., Wilkinson P. N., 1991, *MNRAS*, 251, 54
- Nandra K., George I. M., Mushotzky R. F., Turner T. J., Yaqoob T., 1997, *ApJ*, 477, 602
- Nandra K., Pounds K. A., 1994, *MNRAS*, 268, 405 (NP94)
- Osterbrock D. E., Koski A. T., Phillips M. M., 1975, *ApJ*, 197, L41
- Pounds K. A., 1990, *MNRAS*, 242, 20P
- Pounds K. A., Nandra K., Stewart G. G., George I. M., Fabian A. C., 1990, *Nat*, 344, 132
- Poutanen J., Svensson R., 1996, *ApJ*, 470, 249
- Preuss E., Alef W., Kellermann K. I., 1988, in Reid M. J., Moran J. M., eds., *The Impact of VLBI on Astrophysics and Geophysics*, IAU Symp. 129, Kluwer, Dordrecht, p. 105
- Reynolds C. S., 1997, *MNRAS*, 286, 513
- Sambruna R. M., George I. M., Mushotzky R. F., Nandra K., Turner T. J., 1998, *ApJ*, 495, 749
- Sikora M., Madejski G., Moderski R., Poutanen J., 1997, *ApJ*, 448, 108
- Skibo J. G., Dermer C. D., Kinzer R. L., 1994, 426, L23
- Smith D., Done C., 1996, *MNRAS*, 280, 355
- Smith E. P., et al., 1986, *ApJ*, 306, 64
- Smith E. P., Heckman T. M., 1989, *ApJS*, 69, 365
- Stark A. A., et al., 1992, *ApJS*, 79, 77
- Steinle H., et al., 1997, in Dermer C. D., Strickman M. S., Kurfess J. D., eds, *The 4th Compton Symposium*, AIP, New York, p. 1298
- Struble M. F., Rood H. J., 1987, *ApJS*, 63, 543
- Tanaka Y., Inoue H., Holt, S. S., 1994, *PASJ*, 46, L37
- Turner T. J., George I. M., Mushotzky R. F., Nandra K., 1997, *ApJ*, 475, 118
- Turner T. J., Pounds K. A., 1989, *MNRAS*, 240, 833
- Ubertini P., et al., 1996, *SPIE Proc. Ser.*, 2806, 246
- Urry C. M., Padovani P., 1993, *PASP*, 107, 803
- Véron-Cetty M. P., Véron P., 1993, *ESO Scientific Report*, 13, 1
- Walker R. C., Benson J. M., Unwin S. C., 1988, in Reid M. J., Moran J. M., eds., *The Impact of VLBI on Astrophysics and Geophysics*, IAU Symp. 129, Kluwer, Dordrecht, p. 29
- Walker R. C., Walker M. A., Benson J. M., 1988, *ApJ*, 335, 668
- Walter R., Courvoisier T. J.-L., 1992, *A&A*, 258, 255
- Wamsteker W., Clavel J., 1989, *IAU Circ.*, 4763, 1
- Warwick R. S., Griffiths R. G., Smith D. A., 1998, *MNRAS*, submitted
- Weaver K. A., Arnaud K. A., Mushotzky R. F., 1995, *ApJ*, 447, 121
- White T. R., Lightman A. P., Zdziarski A. A., 1988, *ApJ*, 331, 939
- Williams O. R., et al., 1992, *ApJ*, 389, 157
- Winkler C., 1996, *A&AS*, 120, 637
- Yamashita A., Inoue H., 1996, in Makino F., Mitsuda K., eds., *X-Ray Imaging and Spectroscopy of Cosmic Hot Plasmas*, Univ. Academy Press, Tokyo, p. 313
- Zdziarski A. A., 1998, *MNRAS*, in press
- Zdziarski A. A., Johnson W. N., Done C., Smith D., McNaron-Brown K., 1995, *ApJ*, 438, L63 (Z95)
- Zdziarski A. A., Johnson W. N., Magdziarz P., 1996, *MNRAS*, 283, 193
- Zdziarski A. A., Johnson W. N., Poutanen J., Magdziarz P., Gierliński M., 1997, in Winkler C., Courvoisier T., Durouchoux P., eds., *The Transparent Universe*, ESA SP-382, p. 373
- Życki P. T., Czerny B., 1994, *MNRAS*, 266, 653

This paper has been produced using the Royal Astronomical Society/Blackwell Science  $\LaTeX$  style file.